

Rock ‘n’ Roll Solutions to the Hubble Tension

Prateek Agrawal^{1,2}, Francis-Yan Cyr-Racine^{2,3}, David Pinner^{2,4}, and Lisa Randall²

¹*Rudolf Peierls Centre for Theoretical Physics, University of Oxford, Parks Road, Oxford OX1 3PU, United Kingdom*

²*Department of Physics, Harvard University, 17 Oxford St., Cambridge, MA 02138, USA*

³*Department of Physics and Astronomy, University of New Mexico, 210 Yale Blvd NE, Albuquerque, NM 87106, USA*

⁴*Department of Physics, Brown University, 182 Hope St., Providence, RI 02912, USA*

E-mail: prateek.agrawal@physics.ox.ac.uk, fycr@unm.edu,
randall@physics.harvard.edu

ABSTRACT: Local measurements of the Hubble parameter are increasingly in tension with the value inferred from a Λ CDM fit to the cosmic microwave background (CMB) data. In this paper, we construct scenarios in which evolving scalar fields significantly ease this tension by adding energy to the Universe around recombination in a narrow redshift window. We identify solutions with scalar field potential $V \propto \phi^{2n}$ that have simple asymptotic behavior, both oscillatory (rocking) and rolling. These solutions consistently describe both the field evolution and its fluctuations without approximation. Our findings differ qualitatively from some of the existing literature, which rely upon a coarse-grained fluid description. Combining CMB data with low-redshift measurements, the best fit model has $n = 2$ with a significantly higher value of the Hubble constant as compared to a Λ CDM fit to the same data. Future measurements of the late-time amplitude of matter fluctuations and of the reionization history could help distinguish these models from competing solutions.

Contents

1	Introduction	1
2	Classification of scalar field solutions in cosmology	2
2.1	Emden-Fowler solutions	3
2.2	Exponential potentials	6
2.3	Stability of fluctuations	6
2.4	Comparison with coarse-grained description	7
3	Cosmological Analysis	8
3.1	Parameterization	8
3.2	Datasets	9
3.3	Results: Fixed integer values of n	9
3.4	Results: Promoting n to a free parameter	13
3.5	Results: Comparison with N_{eff}	14
4	Discussion	16
5	Conclusions	19
A	Large Backreaction	20
B	Beyond monomial potentials	21

1 Introduction

The concordance model, Λ CDM, has been very successful in describing the entire observed history of the Universe. But we are now entering the era of precision cosmology where the basic picture can be placed under closer scrutiny. Notably, as the precision of measurements has improved, hints of cracks in the concordance model have appeared. The discrepancy of the present day Hubble parameter H_0 derived from local measurements [1–22] and from cosmic microwave background (CMB) measurements [23–25] is perhaps the most notable indication of a problem. This long-standing deviation (see e.g. refs. [26–30]) has become stronger with time and is currently at a very high statistical significance level [21]. This is worth taking seriously, both for itself and as a template for how we will view current and future cosmological measurements and their potential to probe new physics. While the disagreement may ultimately be explained by experimental systematics (see e.g. refs. [31–39]) or a statistical fluctuation, it is possible that we are seeing the first signs of a theory beyond the standard cosmological model.

Through the positions and spacing of the acoustic peaks present in CMB power spectra, the CMB is sensitive to H_0 via the well-measured angle $\theta_s = r_s/D_M(z_*)$, where r_s is the comoving sound horizon at decoupling, and $D_M(z_*)$ is the comoving angular diameter distance to the surface of last scattering.

The sound horizon is sensitive to early physics, whereas D_M is sensitive to physics after photon-baryon decoupling,

$$r_s = \int_{z_*}^{\infty} \frac{c_s dz'}{H(z')}, \quad (1.1)$$

$$D_M(z) = \int_0^z \frac{dz'}{H(z')}. \quad (1.2)$$

Baryon acoustic oscillation (BAO) data at lower redshifts provide another measurement of r_s/D_M , which asymptotes to $r_s H_0/z$ for small z . This implies that in order to accommodate a value of H_0 that is compatible with the local measurements (and larger than the Planck Λ CDM best fit [25]), r_s has to be modified [40–42].

One simple way to reduce r_s is to increase $H(z)$ before decoupling¹. Since the integral for r_s is dominated by contributions just before the epoch of CMB last-scattering, energy injection around that time is the most efficient in reducing r_s . Indeed, energy injection that is peaked in a narrow window of redshift around recombination minimizes the impact on other successful Λ CDM predictions [41, 42, 47, 48]. Along those lines, there have been a number of studies that try to resolve the Hubble tension by extending Λ CDM by a new energy contribution with distinctive time-dependence and properties (see, e.g., refs. [49–61]). One such scenario, often referred to in the literature as “early dark energy” [62–129], involves a light scalar field whose dynamics can increase $H(z)$ prior to recombination (see ref. [130] for a review).

Evolving scalar fields feature prominently in models of inflation and quintessence (see e.g. refs. [131, 132]). In this paper we present a class of scalar field potentials and solutions which injects energy in the requisite redshift window close to recombination to shrink the sound horizon. We present simple, but exact, solutions that are sufficient to provide the energy injection needed and are under enough control that we can trace their evolution robustly. These solutions arise from potentials of the form $V \propto \phi^{2n}$, with n determining whether the solutions are asymptotically oscillatory or not. In particular, we identify solutions with asymptotically constant equation of state for large n , where there are no oscillatory solutions.

In contrast to some previous analyses (see, e.g., refs. [48, 64, 133]), we use the full equations of motion for the background as well as for the fluctuations, which allows us to show that the coarse-grained approximation used in some past works is not valid near the peak of the energy injection. We will show that these models can fit the CMB and the SH0ES measurement better than Λ CDM, with the power-law index $n = 2$ mildly preferred.

The outline of the paper is as follows. In section 2 we introduce the class of scalar potentials which produce brief energy injections in the early universe. We classify the solutions to the scalar field equations of motion and discuss their stability. In section 3 we describe the procedure we use to fit the models to cosmological data and present the results, comparing to alternate solutions. We highlight unresolved issues in section 4, commenting on their potential resolution, before concluding in section 5.

2 Classification of scalar field solutions in cosmology

CMB data require that the ratio of energy density of the scalar field to the background energy density should peak in a relatively small window in redshift [47, 48, 64]. The goal of this section is to

¹One could also reduce the sound horizon by decreasing the sound speed of the cosmic plasma, or by having hydrogen recombination occur earlier [43–46].

demonstrate potentials that give rise to this behavior.

The energy-momentum tensors for uncoupled fluids are separately covariantly conserved. A consequence of this conservation law is that the ratio of energy densities is determined by the relative equation of state parameters of the scalar field (w_ϕ) and the background (w_b):

$$\frac{\rho_\phi}{\rho_b} \propto \exp\left(-\int 3[w_\phi(a) - w_b(a)]d\ln a\right). \quad (2.1)$$

In order that the energy density in the scalar field does not come to dominate that of the background either at early or late times, $(w_\phi - w_b)$ must transition from negative to positive. This energy injection, which is required to be $\mathcal{O}(10\%)$ in order to resolve the Hubble tension, is localized at the redshift when $w_\phi = w_b$.

One particularly simple class of such solutions has the scalar field initially frozen on its potential, with $w_\phi \approx -1$, before thawing onto a trajectory with a nearly constant equation of state, $w_\phi > w_b$, which we will refer to as rolling solutions. This behavior is in contrast with the familiar case of, *e.g.*, axion dark matter, in which the field and its equation of state oscillate rapidly after thawing. The axion oscillation frequency grows relative to the decreasing Hubble parameter, so that it can become intractable to trace the oscillating field evolution numerically.

Cycle-averaged coarse-graining [134] can provide an accurate description of the fluid at late times, both in the case of axion dark matter as well as more general potentials with oscillating equation of state. However, the coarse-graining approximation does not apply near the initial thawing phase when the field starts oscillating, and this is precisely the regime in which the details of the field evolution and fluctuations have the greatest impact on the gravitational potential, and thence the CMB. Therefore, a cycle-averaged description for such an oscillating solution might be insufficient.

This is why we look for solutions that quickly asymptote to a constant w_ϕ . These have been studied in a different cosmological context in refs. [135–137]. The rolling trajectory is easiest to describe in a simplified limit, in which the background cosmology has a constant equation of state w_b . Further, we work in the approximation where we neglect the back-reaction of the scalar field. This should be justified since the maximal energy injection that we are interested in will be $\mathcal{O}(10\%)$. We emphasize that we use these simplifications to elucidate the physics of the scalar field and do not use them for any of our numerical results.

2.1 Emden-Fowler solutions

We look for a potential such that the late time solution is a trajectory where the scalar field rolls with a constant equation of state, $w_\phi > w_b$,

$$\rho_\phi(a) = \rho_0 \left(\frac{a_0}{a}\right)^{3(1+w_\phi)}. \quad (2.2)$$

Recalling that $1 + w_\phi = a^2 H^2 (\partial_a \phi)^2 / \rho_\phi$, we can extract formulae for $V(\phi)$ and $\partial_a \phi$

$$V(\phi) = \frac{1 - w_\phi}{2} \rho_\phi, \quad (2.3)$$

$$\partial_a \phi = \frac{\sqrt{(1 + w_\phi)\rho_\phi}}{aH}. \quad (2.4)$$

Using $3H^2 M_{\text{Pl}}^2 \approx \rho_b = \rho_{b0} \left(\frac{a_0}{a}\right)^{3(1+w_b)}$, we can solve for $\phi(a)$,

$$\phi(a) = c \left(\frac{a_0}{a}\right)^{\frac{3}{2}(w_\phi - w_b)}, \quad c = \frac{M_{\text{Pl}}}{(w_\phi - w_b)} \sqrt{\frac{4(1 + w_\phi)\rho_0}{3\rho_{b0}}}, \quad (2.5)$$

Asymptotic solutions	Emden-Fowler conditions	Translation to scalar field models	Background	
			Radiation	Matter
Osc. only	$\sigma + 2 \geq 0$	$n \leq \frac{2}{1-w_b}$	$n \leq 3$	$n \leq 2$
Osc. + non-osc.	$\sigma + 2 < 0 \leq \sigma + \frac{\gamma+3}{2}$	$\frac{3+w_b}{1-w_b} \geq n > \frac{2}{1-w_b}$	$5 \geq n > 3$	$3 \geq n > 2$
Non-osc. only	$\sigma + \frac{\gamma+3}{2} < 0$	$n > \frac{3+w_b}{1-w_b}$	$n > 5$	$n > 3$

Table 1. Asymptotics of solutions to the Emden-Fowler equation, and their translation to the parameterization used in this paper. The last two columns give the condition for a given type of solution to exist in either radiation- and matter-dominated cosmologies, respectively.

where we have chosen the additive constant for the solution to correspond to $\phi = 0$ at $a = \infty$. Since both the potential as well as the field have power-law dependence on a , we see that the potential is a power-law in ϕ as well. Explicitly,

$$V(\phi) = \frac{1}{2}(1 - w_\phi)\rho_0 \left(\frac{\phi}{c}\right)^{2n}, \quad n = \frac{1 + w_\phi}{w_\phi - w_b}. \quad (2.6)$$

These ϕ^{2n} potentials have been previously studied in the context of axion models [48, 133] and quintessence [136, 137], but we emphasize that we have arrived at them independently from theoretical motivation by demanding the rolling solutions.

Even when these rolling solutions exist, they may not be the unique solutions. Fortunately, the equation of motion for the ϕ^{2n} potential can be cast into Emden-Fowler form, the solutions of which have been studied in detail (see [138] for a review). The equation of motion of ϕ on a constant w_b background, with back-reaction neglected, is

$$\frac{\partial^2 \phi}{\partial(\log a)^2} + \frac{3}{2}(1 - w_b)\frac{\partial \phi}{\partial(\log a)} + \frac{\partial_\phi V}{H^2(a)} = 0. \quad (2.7)$$

Identifying $s \propto a^{\frac{3}{2}(1-w_b)}$ and $y = s\phi$, the above equation reduces to the Emden-Fowler form,

$$y''(s) + s^\sigma y^\gamma(s) = 0, \quad (2.8)$$

with $\sigma = \frac{4}{1-w_b} - 2(n+1)$ and $\gamma = 2n - 1$. The solutions of Emden-Fowler are characterized by the values of σ and γ . The different regimes of the solution are listed in table 1.

The existence of these rolling trajectories is associated with the fact that $\partial_\phi^2 V(\phi)/H(a)^2$ is an $\mathcal{O}(1)$ constant on these solutions,

$$\frac{\partial_\phi^2 V(\phi)}{H(a)^2} = \frac{9}{4}(1 - w_\phi)(2 + w_\phi + w_b), \quad (2.9)$$

so that the curvature of the potential never grows large relative to the expansion rate of the universe. This should be contrasted with the oscillatory case, *e.g.*, $n = 1$. In this case $\partial_\phi^2 V(\phi)$ is initially much smaller than the expansion rate, and the field is correspondingly stuck on its potential. As the expansion rate decreases, the field begins to roll when $\partial_\phi^2 V(\phi)$ and $H(a)^2$ become comparable, eventually oscillating rapidly at a frequency controlled by $\partial_\phi^2 V(\phi) \gg H(a)^2$. The fact that $\partial_\phi^2 V(\phi)$ never becomes large compared to $H(a)^2$ on the rolling solutions thus prevents the onset of oscillations.

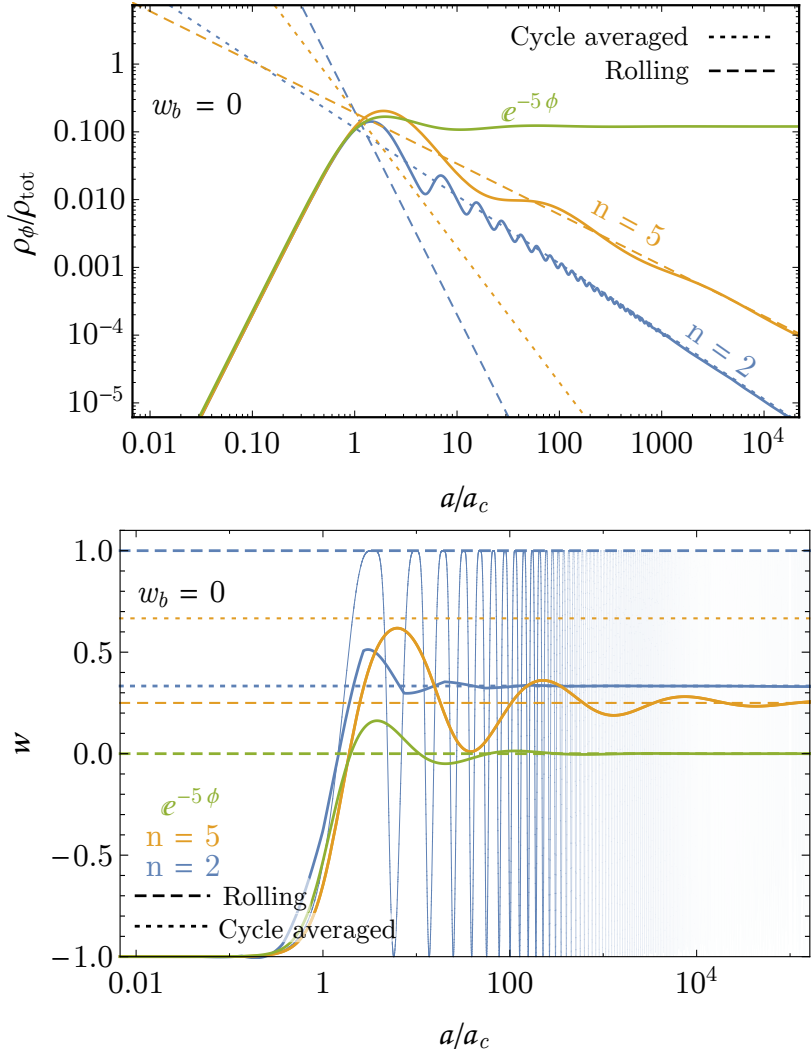


Figure 1. *Top panel:* Evolution of the energy density of the scalar field ϕ relative to total energy density of the universe in a matter-dominated toy cosmology ($w_b = 0$). Here, ρ_{tot} includes the contribution from the scalar field, and a_c denotes the scalar factor at which the field starts rolling. We show the evolution for different choices of n in the scalar potential $V \propto \phi^{2n}$, as well as an example of exponential potential, $V \propto e^{-\lambda\phi}$. We choose values of n to show an example each of an oscillating ($n = 2$) and a rolling solution ($n = 5$). The asymptotics of the numerical solutions is shown to match well with the analytical results derived in the text, neglecting the back-reaction. Note that the presence of slow oscillations around the rolling solution for $n = 5$ is due to the transition from $w_\phi = -1$ to the asymptotic solution; the stability of the rolling solution guarantees that these oscillations are quickly damped. We note that the width of the energy injection grows larger as n is increased. *Bottom panel:* Equation of state of the scalar field as a function of the scale factor for the same potentials as in the left panel. For $n = 2$, the cycle-average of w_ϕ (dark thick blue line) rapidly approaches $w_{\text{osc}} = 1/3$, while for $n = 5$, it asymptotes to the rolling solution with $w_\phi = 1/4$ instead of the cycle-averaged approximation ($w_{\text{osc}} = 2/3$). For the exponential potential, the scalar field approaches the well-known tracking behavior with $w_\phi = w_b$.

The lower bound on n for non-oscillating solutions to exist agrees with the restriction that $w_\phi \leq 1$, given that $n = (1 + w_\phi)/(w_\phi - w_b)$ on the rolling solution. As n is increased above this boundary, both oscillatory and rolling solutions exist simultaneously. However, they are not equally relevant: as we will show in section 2.3, the rolling solutions are unstable whenever both oscillatory and rolling solutions exist. Rapidly oscillating solutions can be modeled by a cycle-averaged description with the effective equation of state given by [48, 134]

$$w_{\text{osc}} \simeq \frac{n-1}{n+1}. \quad (2.10)$$

While tracking these oscillatory solutions could in principle prove problematic for numerical evaluation, in practice these solutions never undergo more than $\mathcal{O}(10)$ s of cycles before the oscillations are cut off. This is because of the transition from matter to dark energy domination in the late Universe. As demonstrated by the boundaries given in table 1, when the background equation of state approaches $w_b \rightarrow -1$, all solutions are non-oscillatory for $n > 1$. As a result, we are able to exactly track these solutions in our numerical results in the following sections, without relying on cycle-averaged approximations.

2.2 Exponential potentials

Exponential potentials are a special limiting case of the rolling solutions which occur when $w_\phi = w_b$, corresponding to the limit $n \rightarrow \infty$. In this case, the field ϕ depends logarithmically on a ,

$$\phi(a) = \phi_0 + \sqrt{\frac{3(1+w_b)\rho_0}{\rho_{b0} + \rho_0}} \log \frac{a}{a_0}, \quad (w_\phi = w_b). \quad (2.11)$$

In this case we have kept the back-reaction of the field since it is possible to obtain a simple analytical solution even with the back-reaction included. This trajectory corresponds to an exponential potential,

$$V(\phi) = V_0 \exp\left(-\lambda \frac{\phi}{M_{\text{Pl}}}\right), \quad \lambda = \sqrt{3(1+w_b) \left(1 + \frac{\rho_{b0}}{\rho_0}\right)}, \quad (w_\phi = w_b). \quad (2.12)$$

On this solution,

$$\frac{\partial_\phi^2 V(\phi)}{H(a)^2} = \frac{9}{2}(1-w_b^2), \quad (w_\phi = w_b) \quad (2.13)$$

is an $\mathcal{O}(1)$ constant, as for the non-oscillatory solutions discussed in the previous subsection. These exponential potentials have previously been studied in the context of quintessence models (see [132] for a review). However, since $w_\phi = w_b$, the energy injection for this potential does not redshift relative to the background (see figure 1), which prevents these solutions from being ideal candidates to resolve the Hubble tension. Therefore we will focus on the case of monomial potentials at finite n for the remainder of the paper.

2.3 Stability of fluctuations

As demonstrated in the previous subsection, for ϕ^{2n} potentials in the range $(3+w_b) \geq n(1-w_b) > 2$, rolling solutions are irrelevant at late times, since the field redshifts more quickly than the oscillation amplitude. In fact, the rolling solutions are unstable for this range of n . The homogeneous equation

of motion for linear fluctuations about the rolling solution, written using $\log a$ as the time variable and assuming a background equation of state w_b , is

$$\frac{\partial^2 \delta\phi_k}{\partial(\log a)^2} + \frac{3}{2}(1-w_b)\frac{\partial\delta\phi_k}{\partial(\log a)} + \left[\frac{k^2}{a^2 H(a)^2} + \frac{9}{4}(1-w_\phi)(2+w_\phi+w_b) \right] \delta\phi_k = 0. \quad (2.14)$$

It has solutions which scale as

$$\delta\phi_0 \sim a^{-\frac{3}{4}[(1-w_b) \pm \sqrt{4w_\phi^2 + (1+w_b)(4w_\phi+w_b-7)}]}. \quad (2.15)$$

For $w_\phi < \sqrt{2}\sqrt{1+w_b} - (1+w_b)/2$, these solutions are oscillatory, and their envelope redshifts as $a^{-3(1-w_b)/4}$, while the rolling solution redshifts as $a^{-3(w_\phi-w_b)/2}$. Thus the fluctuations grow relative to the rolling solution for $1 > w_\phi > (1+w_b)/2$, corresponding to $2 < n(1-w_b) < 3+w_b$ and coinciding with the entire range of n for which both oscillatory and rolling solutions exist. For larger n , these fluctuations redshift more quickly, and the rolling solutions are stable.

The oscillatory solutions, on the other hand, exhibit a somewhat more subtle instability. For $n > 1$, $\partial_\phi^2 V \propto \phi^{2(n-1)}$ vanishes as $\phi \rightarrow 0$. During each cycle of the oscillation, the fluctuations of the ϕ field become massless, leading to a short burst of particle production. If the growth rate of the instability is sufficiently large, $\partial_\phi^2 V \gg H^2$, the field will eventually fragment completely into modes with $k > 0$ [139, 140], invalidating the linear perturbation theory used in our analysis.

On the oscillating solutions,

$$\left. \frac{\partial_\phi^2 V}{H^2} \right|_{osc} \propto a^{-\frac{3}{n+1}(n(1-w_b)-3-w_b)}, \quad (2.16)$$

so that the growth rate increases with scale factor for $n < (3+w_b)/(1-w_b)$. The case of $w_b = 0$ is most relevant for our numerical results, since the shape of the energy injection constrains most of the oscillations to occur during matter domination. For $n = 3$, the growth rate of the fluctuations remains smaller than the expansion rate at all times, so that they never become important. For $n = 2$, however, the growth rate accelerates, and it is a numerical question whether these fluctuations become important before the onset of dark energy domination, at which point the background solutions cease to be oscillatory. Of course, a realistic potential may include a mass term for the scalar field which could prevent this instability entirely². For our results in the following sections, we have not included such a mass term; rather, we have simply checked numerically that the scalar field fluctuations remain under control.

2.4 Comparison with coarse-grained description

The oscillatory solutions have a frequency which monotonically increases relative to the Hubble expansion rate, which makes it numerically challenging to track their evolution to late times. The usual method for addressing this issue is to coarse-grain these solutions, along with their fluctuations, replacing the numerically computed equation of state and rest-frame sound speed by their cycle-averaged values [48, 134],

$$w_{osc} \simeq \frac{n-1}{n+1}, \quad \langle c_s^2 \rangle \simeq \frac{2a^2(n-1)\omega^2 + k^2}{2a^2(n+1)\omega^2 + k^2}, \quad (2.17)$$

²From a model-building perspective, such a mass term would need to be stabilized against UV corrections by, for example, a shift-symmetry.

in which ω is the instantaneous oscillation frequency of the field fluctuations. As demonstrated in figure 1, however, this description is inaccurate near the onset of thawing, when the ratio of energy density of the scalar field to that of the background is near its maximum. In fact, we will see (figure 3 below) that the oscillating solutions go through a short period of kination ($w \approx 1$) during the first oscillation cycle, rapidly depleting their energy density relative to the cycle-averaged solution. For $n = 2$ and $w_b = 0$, it takes several oscillation cycles before the oscillation frequency becomes large relative to the Hubble rate, at which point $\rho_\phi/\rho_{\text{tot}}$ has dropped by more than two orders of magnitude relative to its $\mathcal{O}(10\%)$ maximum.

The fluctuations are similarly poorly described by coarse-graining. At the onset of thawing, $\partial_\phi^2 V \simeq H^2$, so that all subhorizon modes have $k^2 \gtrsim \partial_\phi^2 V$. Thus the fluctuations are kinetic energy dominated, and their rest-frame sound speed is close to 1 for the entire relevant range of scale factors and k -modes. By contrast, taking the above cycle-averaged formula gives $\langle c_s^2 \rangle \rightarrow w_{\text{osc}} < 1$ over a large range of k , since ω becomes large relative to H at late times. The detailed evolution of these fluctuations qualitatively affects the fit of these scalar field models to the CMB data; therefore, in our numerical study, we have chosen not to make any coarse-graining approximations. For the following results, we have tracked the individual oscillations to late times, checking that numerical errors remain under control until the energy density of the scalar field is sufficiently subdominant.

3 Cosmological Analysis

3.1 Parameterization

In this section we present the fits for the models above to the cosmological data. We use the following parametrization for the model,

$$V(\phi) = V_0 \left(\frac{\phi}{M_{\text{Pl}}} \right)^{2n} + V_\Lambda, \quad (3.1)$$

where V_Λ is a constant. In addition to V_0 , V_Λ , and n , the scalar field initial conditions ϕ_i and $\partial_a \phi_i$ are the two other free parameters. Since we are primarily interested in field solutions that are initially frozen, we will always set the velocity of the scalar field to zero at very early times. Given $\phi_i \sim M_{\text{Pl}}$ initial conditions, the field will then begin to thaw when $V_0 \sim \rho_b$. Thus in order that the field begins to roll near matter-radiation equality, we must have $V_0 \sim \text{eV}^4$. Note that the smallness of the dimensionless coupling, $(\text{eV}/M_{\text{Pl}})^4$, is consistent with a softly broken shift symmetry (from e.g. instantons) and therefore technically natural, similar to the case of the $\Lambda_{\text{QCD}}^4 \cos(a/f_a)$ potential for the QCD axion. For a discussion of the tuning required to explain the absence of additional couplings, see section 4. In our model, the value of V_Λ determines the late-time dark energy density, and its value is set by demanding that the Universe is spatially flat. The parameter n determines the shape of the energy injection. We note that eq. (3.1) completely determines the evolution of the scalar field and its perturbations. In particular, there is no extra freedom to independently change the sound speed of the scalar field perturbations in this model.

In principle, we could perform our Markov Chain Monte Carlo (MCMC) analysis in terms of V_0 and ϕ_i . However, since our preliminary analysis shows that cosmological data are primarily sensitive to both the timing and the amount of energy injected by the rolling scalar field, we choose to parametrize the model using the approximate redshift at which the field starts rolling, $z_{c,\text{MC}}$, and the approximate fraction of energy injected by the scalar field $f_{\phi,\text{MC}} \approx (\rho_\phi/\rho_{\text{tot}})|_{\text{max}}$. The initial field value ϕ_i and the V_0 parameter are then determined through the relations $\partial_\phi^2 V(\phi_i) \equiv 9H^2(z_{c,\text{MC}})$ and $V(\phi_i) \equiv$

$3f_{\phi,\text{MC}}H^2(z_{c,\text{MC}})M_{\text{Pl}}^2$. These latter relations should be interpreted as the definitions of $z_{c,\text{MC}}$ and $f_{\phi,\text{MC}}$.

We implement this model into a modified version of the `Class` code [141, 142]. We perform parameter scans over $f_{\phi,\text{MC}}$ and $\ln(1+z_{c,\text{MC}})$ as well as the standard six flat Λ CDM parameters using the `MontePython` [143, 144] software package version 3.1³. We use flat prior distributions on our scalar field parameters, $f_{\phi,\text{MC}} \in [10^{-4}, 0.3]$ ⁴ and $\ln(1+z_{c,\text{MC}}) \in [7.5, 9.5]$, and the same prior distributions for the other cosmological parameters as in the Planck analysis [24]. We solve both the background and perturbed Klein-Gordon equations at each step to obtain the exact cosmological evolution of the scalar field and its perturbations, and use this solution to determine a posteriori the exact maximum fraction of energy injected by the rolling field, f_{ϕ} , as well as the critical redshift z_c at which the energy injection peaks. In the following, we shall present our results in terms of these latter exact quantities.

3.2 Datasets

In our cosmological analysis, we use the following datasets⁵:

- **Planck:** We use the Planck 2015 CMB temperature and polarization likelihoods [146] for both low- ℓ and high- ℓ , including all nuisance parameters and using the same prior distributions as in the Planck analysis [24] for those. We also include the Planck lensing likelihood [147].
- **BAO:** We include baryon acoustic oscillation (BAO) measurements from the CMASS and LOWZ galaxy samples of the Baryon Oscillation Spectroscopic Survey (BOSS) DR12 [148]. These include both line-of-sight and transverse BAO measurements, as well as constraints on the growth of structure through the parameter $f\sigma_8$. We shall refer to these datasets as high- z BAO. We also include low- z BAO measurements from the 6dF Galaxy Survey [149] and from the Main Galaxy Sample (MGS) of SDSS [150].
- **SH0ES:** We include the measurement [5] of the local Hubble parameter $H_0 = 73.52 \pm 1.62$ km/s/Mpc⁶.
- **Pantheon:** We include the Pantheon compilation of type Ia supernovae (SN Ia) [153], which includes 1048 luminosity distances in the redshift range $0.01 < z < 2.3$. We include in our fit the nuisance parameter M describing the fiducial absolute magnitude of a SN Ia.

3.3 Results: Fixed integer values of n

We show posterior distributions for the most relevant parameters in figure 2 for $n = 2, 3$, and 4. The most striking feature is the similarity of the different distributions as n is changed, with the notable exception of the injected energy fraction f_{ϕ} . Of the models shown, the $n = 2$ (corresponding to $V(\phi) \propto \phi^4$) posterior stands out for being more highly weighted towards larger values of the energy injection, which results in slightly larger values of the Hubble constant being preferred. Indeed, the

³This was the most-recent version available at the onset of the work.

⁴We set a prior on $f_{\phi,\text{MC}}$ rather than its logarithm to avoid volume effects at low $f_{\phi,\text{MC}}$ values (see e.g. refs. [87, 109, 113, 123, 145]). The lower bound is chosen to avoid numerical instabilities arising when $f_{\phi,\text{MC}} = 0$ while allowing the model to essentially reduce to Λ CDM in this limit.

⁵These datasets were the latest available at the time the analysis was performed.

⁶As discussed in refs. [151, 152], using a Gaussian prior on H_0 can lead to inconsistencies when considering cosmological models that differ significantly from Λ CDM at late times. Since the models considered here primarily affect cosmology at early times, we can safely use a Gaussian prior on H_0 .

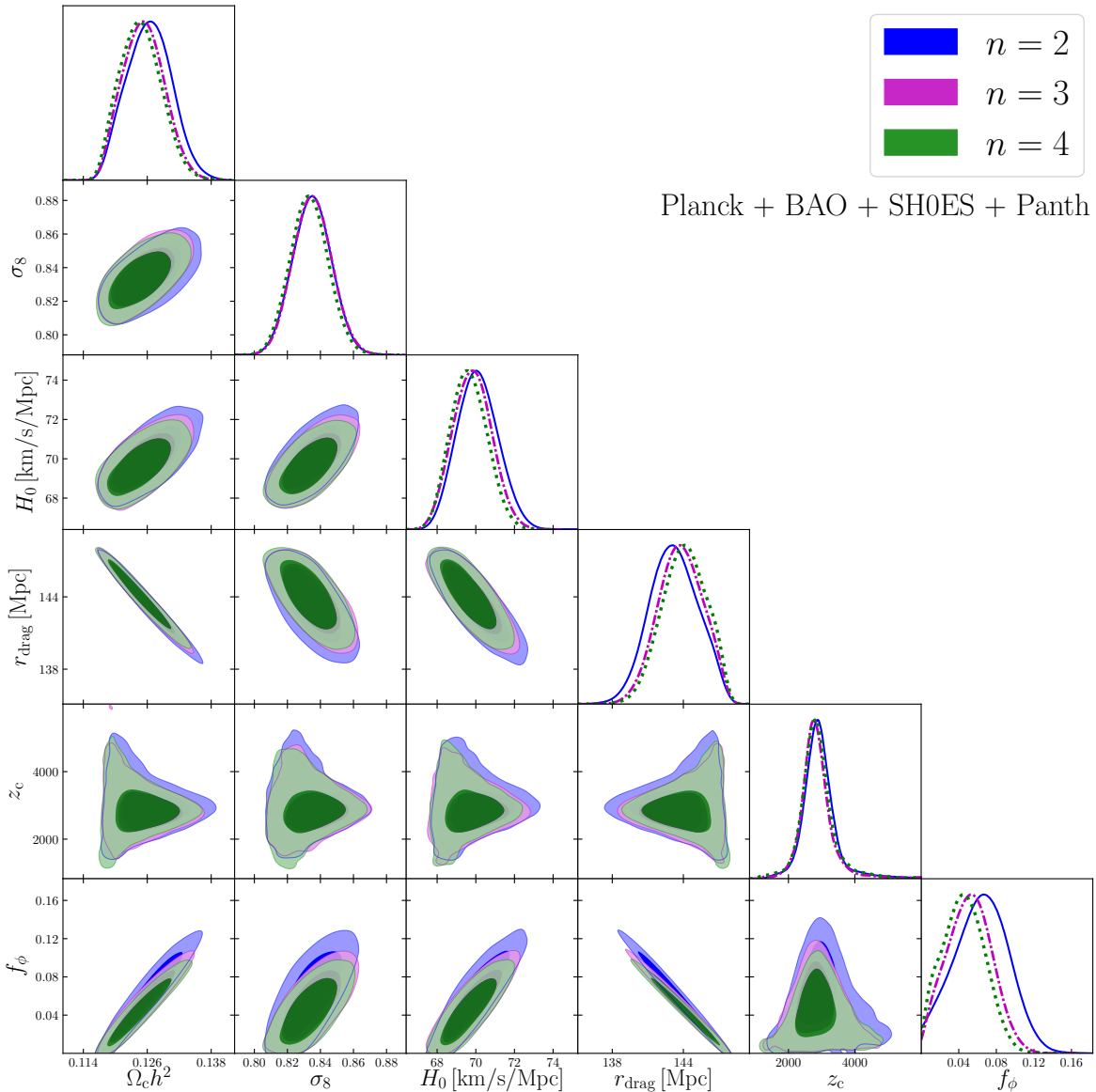


Figure 2. Marginalized posterior distributions for $V \propto \phi^{2n}$ models for three different values of n . Results are shown here for the data combination “Planck + BAO + SH0ES + Pantheon”.

inclusion of the SH0ES data in the analysis leads to a nearly 2σ preference for a nonzero energy injection around $z_c \simeq 3100$. As per our discussion in section 1 (see also ref. [41]), the size of the baryon-photon sound horizon at the drag epoch r_{drag} is strongly anti-correlated with the injected energy fraction f_ϕ . This smaller sound horizon is the main driver behind the reduction of the Hubble constant tension in these models.

The physical dark matter density ($\Omega_c h^2$) is strongly correlated with f_ϕ in order to obtain the correct early integrated Sachs-Wolfe effect [154], which fixes, in part, the height of the first CMB temperature acoustic peak. This larger dark matter abundance, combined with the extra energy

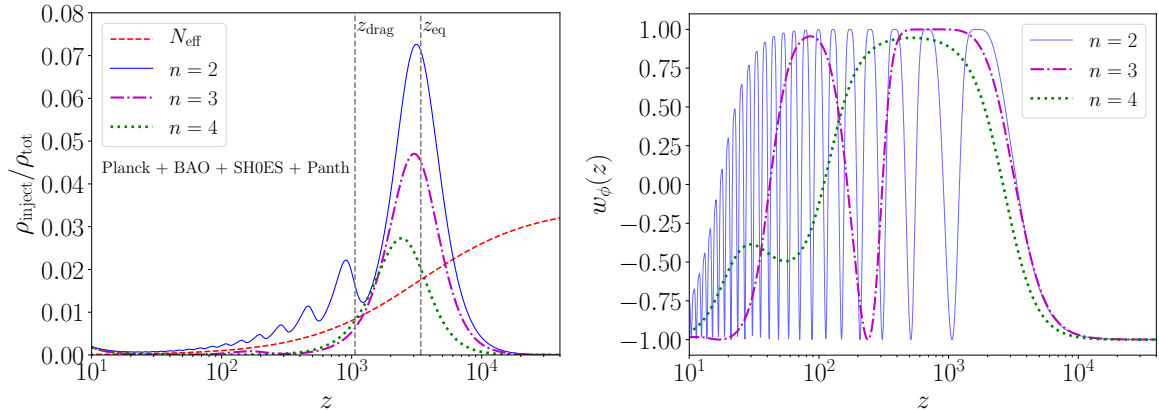


Figure 3. *Left panel:* Energy injection profile for the best-fit models for each value of n as a function of redshift. Results are shown here for the data combination “Planck + BAO + SH0ES + Pantheon”. For reference, we also show the amount of energy injected as compared to standard Λ CDM for the best fit N_{eff} model using the same data combination (corresponding to $\Delta N_{\text{eff}} = 0.27$). To guide the eye, we have indicated by vertical dashed lines the matter-radiation equality and baryon drag epochs in the standard Λ CDM model. *Right panel:* The scalar field equation of state as a function of redshift for each value of n .

injected by the rolling scalar field, leads to an increase of the CMB Silk damping scales as compared to the baryon-photon sound horizon since $r_{\text{damp}}/r_s \propto H^{1/2}$ [155]. This is compensated in the CMB fit by increasing the values of both the scalar spectral index n_s and fluctuation amplitude A_s as compared to their Λ CDM values. As a consequence of this change to the primordial spectrum of scalar perturbations, the late-time amplitude of matter fluctuations as probed by the σ_8 parameter are increased. Thus, obtaining a larger Hubble parameter within these scalar field models is correlated with an increase in the σ_8 value. This is a generic feature of models that inject energy near recombination, which might lead them to be in tension with late-time measurements of the matter power spectrum (see e.g. ref. [156]). We shall come back to this point in the discussion.

We show in figure 3 the best-fit energy-injection profile and the EoS of the scalar field for each value of n we consider. We observe that, for a fixed width of the primary energy injection peak, models with lower values of n allow for more energy to be injected, resulting in a smaller value of the baryon-photon sound horizon and larger Hubble constant. However, as explained in section 2, these low- n models also have strong oscillatory solutions with secondary energy injection peaks post recombination, which adversely affect the fit to CMB data. On the other hand, as was shown in figure 1, models with large values of n have a broader primary energy injection peak and slowly decaying tail, which means that it is difficult for these models to inject sufficient energy prior to recombination while not having significant residual energy towards low redshifts. The fit to cosmological data is thus driven by the competing effects of injecting the largest possible amount of energy in a relatively narrow window prior to recombination, while at the same time being able to get rid of this energy as quickly as possible in the post-recombination era. In contrast with the results of section 2.1, which were derived in a toy cosmology with $w_b = 0$, the best-fit solutions for $n = 3$ and $n = 4$ never achieve their asymptotic equations of state due to the effect of the cosmological constant at late times. The salient feature, however, is the relatively large instantaneous value of $w_\phi \approx 1$ obtained shortly after the peak of the energy injection for all values of n . This causes most of the energy density to quickly redshift away,

Datasets	Λ CDM	$n = 2$	$n = 3$	$n = 4$	N_{eff}
<i>Planck</i> high- ℓ	2439.0	2440.4	2440.0	2440.5	2442.0
<i>Planck</i> low- ℓ	10495.8	10494.3	10494.4	10494.6	10494.5
<i>Planck</i> lensing	9.5	10.0	10.2	10.0	9.6
BAO - low z	1.6	1.6	1.5	1.5	2.1
BAO - high z	1.8	1.9	1.9	1.9	1.9
Pantheon	1027.0	1027.0	1027.0	1027.0	1026.9
SH0ES	11.4	3.2	4.5	4.9	5.1
Total χ^2_{min}	13986.1	13978.3	13979.5	13980.3	13982.1
$\Delta\chi^2_{\text{min}}$	0	-7.8	-6.6	-5.8	-4.0

Table 2. Best-fit χ^2 values for each individual dataset used in our cosmological analysis.

so that the fit is relatively insensitive to the subsequent dynamics. The speed of the transition from $w_\phi \simeq -1$ to $w_\phi \simeq 1$ determines the width of the energy injection; as shown in figure 3, this width is minimized at small n .

The finding that lower n values provide a better fit to cosmological data is supported by examining the individual best-fit χ^2 values. We present these in table 2 for $n = 2, 3$, and 4, as well as for Λ CDM⁷. We find that the $n = 2$ model provides that best overall improvement of the fit as compared to Λ CDM. We observe, however, that the improved fit to the SH0ES measurement of H_0 is partially offset by a degradation of the goodness-of-fit to the high- ℓ CMB tail and to the CMB lensing spectrum. We note that the results shown in table 2 are significantly different than those presented in ref. [64] due to their use of a coarse-grained effective fluid approach. As discussed in section 2 above, the coarse-grained approach is a reasonable approximation for $n = 2$ deep in the matter-dominated era (see right panel of figure 3 for $z < 500$), but it fails to accurately capture the most important part of scalar field evolution near the peak of the energy injection. The coarse-grained approach is inaccurate for $n \geq 3$ since the models undergoes at most two oscillations before the onset of dark energy domination, resulting in very different fits once the exact evolution of the scalar field is taken into account.

We show in table 3 the mean, 1σ uncertainty, and best fit values for the most relevant cosmological parameters and quantities. The $n = 2$ best-fit model has the largest Hubble constant value of all models studied in this paper, which is a direct consequence of it having the largest energy injection fraction (see figure 3), and therefore the smallest photon-baryon drag horizon. The physical dark matter density is also significantly larger for the $n = 2$ best-fit model, as is the amplitude of the matter power spectrum as captured through the σ_8 parameter, for reasons explained above. We will perform a thorough comparison between the $n = 2$ model and N_{eff} in section 3.5 below.

In figure 4, we show the CMB residuals between our best-fit ϕ^{2n} , Λ CDM, and N_{eff} models using the data combination “Planck + BAO + SH0ES + Pantheon”, and a reference Λ CDM model fitted to “Planck + BAO + Pantheon” data. This allows us to isolate the impact of the SH0ES data on the residuals. All models shown display, on average, less power in C_ℓ^{TT} at $\ell > 500$ compared to our reference Λ CDM model. This is caused by the well-known [155] competition between having a large enough Hubble constant to fit the SH0ES measurement while ensuring that there is enough power in the CMB temperature Silk damping tail. We note, however, that the variations between the different models shown are typically smaller than the size of the error bars.

⁷These χ^2 values were obtained by running a steepest-gradient minimizer on the relevant likelihoods.

Parameter	Λ CDM	$n = 2$	N_{eff}
$100 \Omega_b h^2$	2.238 (2.234) $^{+0.014}_{-0.015}$	2.261 (2.270) $^{+0.021}_{-0.020}$	2.254 (2.253) ± 0.018
$\Omega_c h^2$	0.1180 (0.1182) ± 0.0012	0.1264 (0.1284) $^{+0.0044}_{-0.0043}$	0.1220 (0.1227) $^{+0.0027}_{-0.0028}$
$100 \theta_s$	1.0420 (1.0419) ± 0.0003	1.0415 (1.0414) ± 0.0004	1.0414 (1.0413) $^{+0.0004}_{-0.0005}$
τ_{reio}	0.074 (0.072) $^{+0.013}_{-0.012}$	0.072 (0.074) $^{+0.013}_{-0.012}$	0.075 (0.073) $^{+0.013}_{-0.012}$
$\ln(10^{10} A_s)$	3.079 (3.074) $^{+0.024}_{-0.021}$	3.091 (3.097) $^{+0.026}_{-0.023}$	3.089 (3.087) $^{+0.025}_{-0.022}$
n_s	0.968 (0.966) ± 0.004	0.978 (0.966) ± 0.007	0.977 (0.980) $^{+0.006}_{-0.007}$
$f_\phi / \Delta N_{\text{eff}}$	-	0.064 (0.080) $^{+0.031}_{-0.028}$	0.26 (0.29) ± 0.16
z_c	-	3040 (2902) $^{+330}_{-630}$	-
σ_8	0.819 (0.817) $^{+0.009}_{-0.008}$	0.835 (0.840) ± 0.012	0.831 (0.831) ± 0.011
Ω_m	0.304 (0.305) ± 0.007	0.304 (0.304) ± 0.007	0.299 (0.299) $^{+0.007}_{-0.008}$
r_{drag} [Mpc]	147.6 (147.6) ± 0.3	143.2 (142.1) $^{+2.0}_{-2.3}$	145.1 (144.8) ± 1.5
H_0 [km/s/Mpc]	68.2 (68.0) ± 0.5	70.1 (70.6) $^{+1.0}_{-1.2}$	69.7 (69.9) ± 1.1

Table 3. Mean values and 68% confidence intervals for key cosmological parameters using the data combination “Planck + BAO + SH0ES + Pantheon”. The numbers in parentheses are the best-fit values for each model.

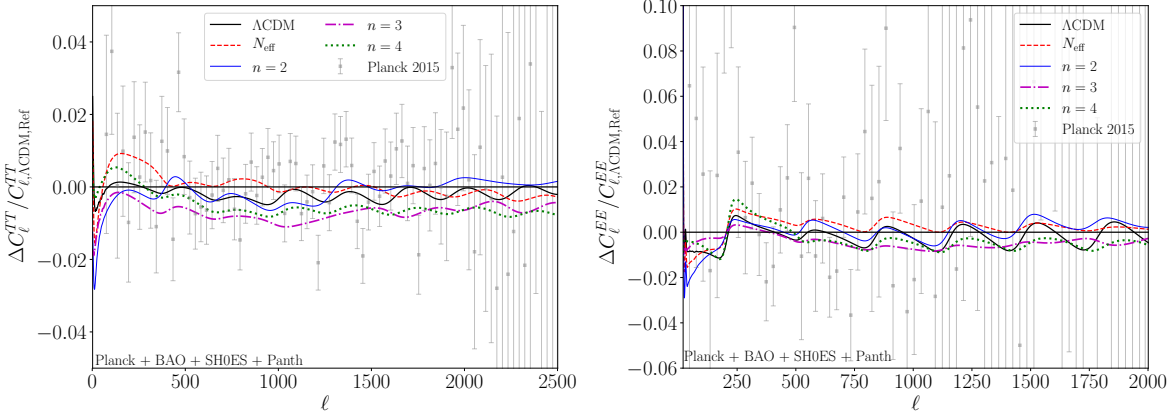


Figure 4. High- ℓ CMB residuals between the “Planck + BAO + SH0ES + Pantheon” best fit models for Λ CDM, N_{eff} , and ϕ^{2n} , and a best-fit Λ CDM reference model obtained using the data combination “Planck + BAO + Pantheon”. The left panel shows the temperature residuals, while the right panel shows the E-mode polarization residuals.

3.4 Results: Promoting n to a free parameter

So far, we have considered only fixed integer values of the power-law index n parameterizing the scalar potential. This was effectively restricting the behavior of the energy injection to have a specific shape specified by our choice of n . In this section, we relax the assumption of fixed integer values of n and allow the power-law index to float freely in the fit to cosmological data (writing our potential as $V \propto |\phi|^{2n}$), hence exploring a broader range of energy injection shapes and scalar field behaviors. While we adopt this simple phenomenological point-of-view, we note that models with noninteger n values may be problematic from a model-building perspective as they typically correspond to nonlocal theories (see e.g. ref. [157]). We consider a flat prior on $n \in [2, 6]$. The main results of this analysis are shown in figure 5. As discussed above, the data tends to favor lower values of the index n since they

allow a larger peak energy injection fraction. The right panel clearly illustrates that larger Hubble constant values are more likely for the lowest possible index n , which, given our choice of priors, corresponds to $n \sim 2$ (that is, $V \propto \phi^4$).

Figure 5 suggests that one should consider even lower values of n in order to fit the large Hubble constant from the SH0ES measurement, despite these solutions being increasingly oscillatory. To explore this possibility, we extend our prior range on n to include values all the way down to $n = 1.5$, a compromise between exploring low values of n while at the same time ensuring that the oscillatory solutions are tractable numerically. We find that it is indeed possible to obtain larger values of the Hubble constant (our best fit with $n < 2$ has $H_0 = 71.74$ km/s/Mpc for $n = 1.89$), but at the price of significantly degrading the fit to the CMB damping tail. Overall, we find that none of the models with $n < 2$ provides a better global fit to cosmological data than the $n = 2$ model presented in tables 2 and 3.

3.5 Results: Comparison with N_{eff}

It is informative to compare the scalar field models with the more standard N_{eff} extension to the Λ CDM model. The amount of energy injected by the best-fit N_{eff} model is shown in figure 3 (corresponding to $\Delta N_{\text{eff}} = 0.27$). The addition of relativistic species leads to a broadband energy injection, in contrast to the relatively narrow energy injection peaks of the $n = 2$ model. Despite these differences, we see in table 2 that the fit to the high- ℓ CMB data is similar to the $n = 2$ scalar field model. We note however that these two fits are significantly worse than that achieved in the reference Λ CDM model fitted only to “Planck + BAO + Pantheon.” The main difference between the two models is the physical amount of dark matter required to obtain the correct magnitude of the early ISW effect. Since the N_{eff} model injects less relativistic energy near matter-radiation equality than the $n = 2$ model, a smaller amount of dark matter is required to leave the early ISW effect invariant. In turn, this leads to a smaller Ω_m than in $n = 2$, which worsens the fit to late-time probes such as BAO. Thus, while N_{eff} models can accommodate larger values of the Hubble constant without degrading the global fit, they do so by compromising the fit to the low- z BAO data as shown in the last column of table 2.

By comparison, the $n = 2$ scalar field model has a similar fit to the CMB high- ℓ tail as the N_{eff}

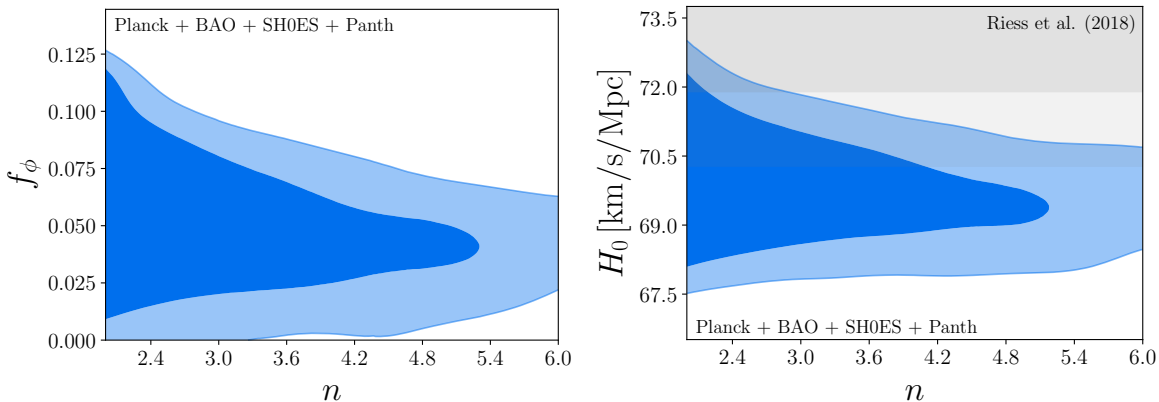


Figure 5. Marginalized posterior in the f_ϕ - n plane (left panel), and the H_0 - n plane (right panel). The gray band shows the SH0ES measurement [5]. Results are shown here for the data combination “Planck + BAO + SH0ES + Pantheon.” Clearly, larger values of the Hubble constant require lower values of n .

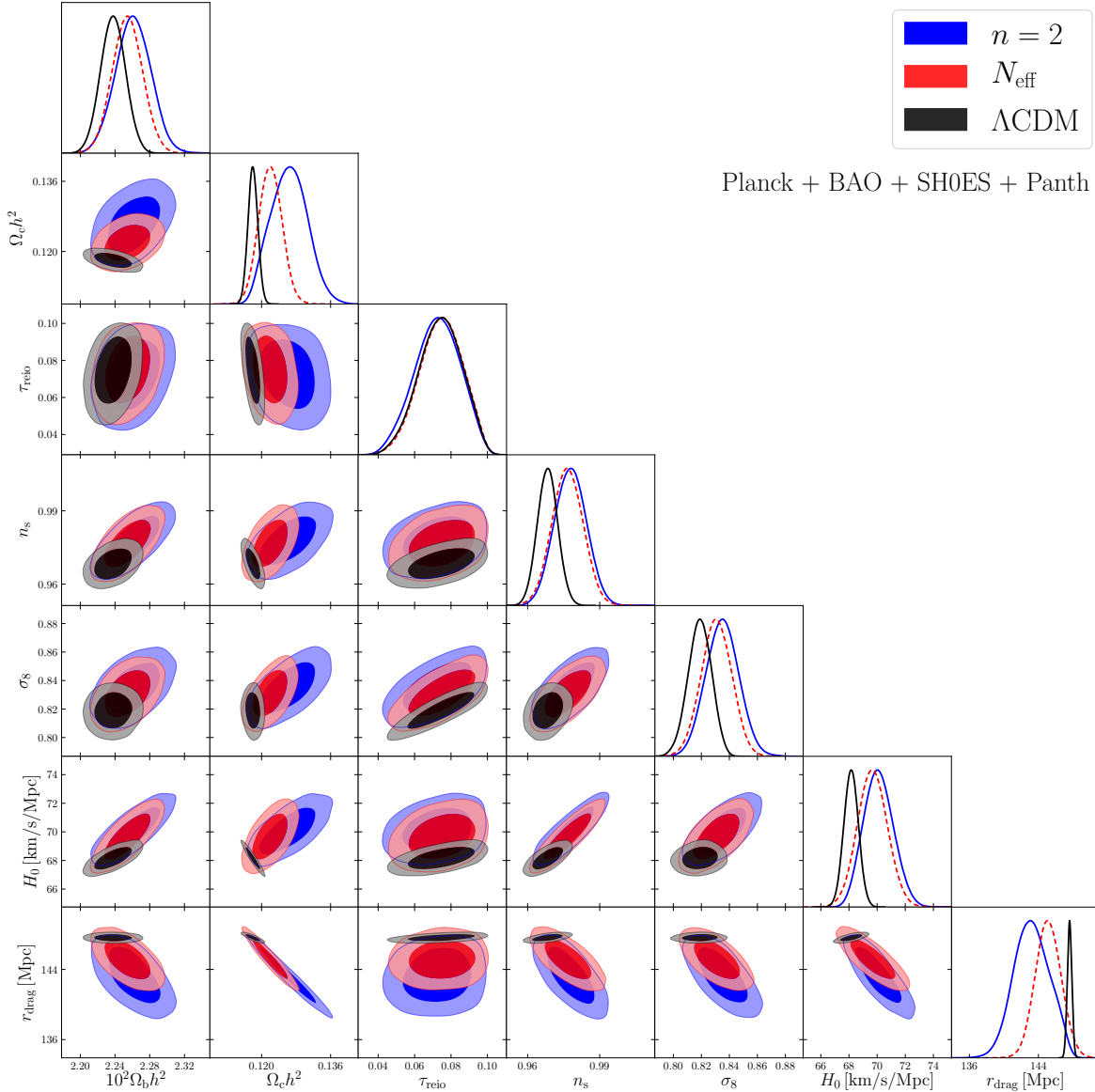


Figure 6. Comparison between the $n = 2$ model, the N_{eff} extension of the standard cosmological model, and plain ΛCDM . All posterior distributions shown here were obtained using the data combination “Planck + BAO + SH0ES + Pantheon”.

model, while at the same time typically allowing for larger Hubble constant and better fit to BAO data. We must however keep in mind that the ϕ^{2n} models introduce two free parameters (f_ϕ, z_c) to the fit, compared to the single parameter in N_{eff} models. We can use the Aikake information criterion (AIC) [158], which can be defined as $\Delta\text{AIC} = \Delta\chi^2_{\text{min}} + 2\Delta k$, where Δk is the difference in the number of free parameters between the two models considered. Using the ΛCDM fit to the “Planck + BAO + SH0ES + Pantheon” dataset as our reference model, we obtain $\Delta\text{AIC}_{n=2} = -2.9$, while $\Delta\text{AIC}_{N_{\text{eff}}} = -2.4$, indicating that the $n = 2$ scalar field model provides a slightly better fit to the data as compared to

N_{eff} , even after accounting for the extra free parameter. In comparison, the $n = 3$ and the $n = 4$ models provide a worse global fit to the data than N_{eff} after accounting for the different numbers of free parameters. This reinforces the fact that models with lower values of the power-law index n are favored by the data. On the other hand, N_{eff} models are theoretically somewhat simpler. UV completions of ϕ^{2n} models must explain not only the absence of additional self-couplings, but also the surprising coincidence between the timing of the energy injection and the redshift of matter-radiation equality demanded by the fit to CMB data.

A quantitative comparison between the $n = 2$ scalar field model and the N_{eff} extension of Λ CDM is shown in figure 6. We first observe that the scalar field model generally allows for smaller values of the baryon drag horizon r_{drag} than the N_{eff} model. Naively, following the argument presented in ref. [41], this should allow the scalar field model to accommodate a larger Hubble constant as compared to N_{eff} . Instead, we see that the two models have fairly similar posterior distribution for H_0 , with the scalar field model allowing only slightly larger values of the expansion rate. This difference between our naive expectation and what is shown in figure 6 is caused by the different amount of dark matter needed in each model, as described above. This larger dark matter abundance pulls down on the Hubble constant value in the cosmological fit, partially compensating for the increase coming from a smaller baryon sound horizon. The scalar field models with ϕ^{2n} potentials are thus less efficient at turning a given reduction of the sound horizon into an increase of H_0 , as compared to N_{eff} .

Both $n = 2$ and N_{eff} models have larger values of σ_8 which are largely caused by the change to the primordial spectrum of fluctuations (A_s and n_s) necessary to bring the CMB damping tail in agreement with the data. As discussed in section 3.3, this is a generic feature of models that inject energy near the epoch of recombination. The effect is larger for the $n = 2$ model since more energy is injected overall, leading to a slightly larger value of σ_8 as compared to N_{eff} .

4 Discussion

We have seen that a scalar field with $V \propto \phi^{2n}$ leads to an energy injection which is localized in time, potentially alleviating the tension between local measurements of the Hubble constant and that inferred from CMB observations. One important worry is the slight degradation of the fit to CMB data when Planck and SH0ES measurements are analyzed simultaneously. Does this indicate that Planck data alone disfavors the energy injection brought by the rolling scalar field? To answer this question, we redo our MCMC analyses for the ϕ^{2n} models but this time without the SH0ES likelihood. In figure 7 we show the normalized posterior of H_0 resulting from these analyses for Λ CDM, N_{eff} , and $n = 2$. While both the $n = 2$ and N_{eff} posteriors are wider than Λ CDM, that of $n = 2$ is peaked at marginally higher values of H_0 than either alternative model, with N_{eff} actually peaking below Λ CDM. This suggests that the energy injection brought by the evolving scalar field can naturally accommodate larger Hubble constants in the CMB fit, even without prior information from late-time measurements. While the $n = 2$ model does not entirely remove the H_0 tension, it can significantly reduce it to the $\sim 2\sigma$ level. Given the longer tail of the posterior distribution, future local measurements of H_0 which reduce the error bars could more strongly distinguish the scalar field model from N_{eff} .

It is also interesting to examine the impact of the ϕ^{2n} models on late-time cosmology. We show in figure 8 the changes to the cosmology at $z < 1$ for the different models studied in this paper. The left panel shows the fit to the BAO measurements used in our analyses. For clarity, we illustrate the quantity $D_V(z)/r_{\text{drag}}$ for the best-fit parameters of the different models considered, normalized by that of the “Planck + BAO + Pantheon” Λ CDM model. We see that all models have lower values of

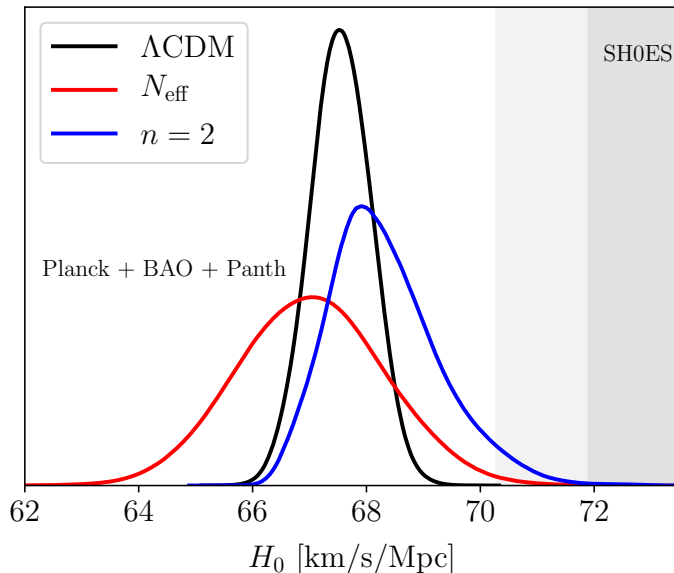


Figure 7. Normalized H_0 posteriors obtained using the data combination “Planck + BAO + Pantheon”, that is, without including the local Hubble constant measurement from ref. [5].

$D_V(z)/r_{\text{drag}}$ over the redshift range shown. Expanding around $z = 0$,

$$\frac{D_V(z)}{D_{V,\text{fid}}(z)} \approx \frac{H_{0,\text{fid}}}{H_0} [1 + (\Omega_{\text{m},\text{fid}} - \Omega_{\text{m}})z + \mathcal{O}(z^2)]. \quad (4.1)$$

In all of the models considered, Ω_{m} is decreased relative to the best-fit “Planck + BAO + Pantheon” ΛCDM reference model, despite the relative increase in $\Omega_{\text{c}}h^2$. This produces a positive slope for the D_V ratio at late times, guaranteeing that those models which fit the high- z BAO data at redshift 0.5 will be in mild tension with the MGS measurement at lower redshift. Since N_{eff} has the smallest Ω_{m} of all models shown, this effect is more severe for this model.

The right panel of figure 8 shows the Hubble expansion history at $z < 1$ for our best-fit $n = 2$ model, and compares it to that of the best-fit ΛCDM and N_{eff} models (for the data combination “Planck + BAO + SH0ES + Pantheon”). To illustrate how the scalar field model helps reconciling the CMB, BAO, and SH0ES measurements of the expansion rate, we also show two sets of line-of-sight BOSS DR12 BAO measurements [148]. The first set is calibrated using the sound horizon from $n = 2$ scalar field fit to the CMB ($r_{\text{drag}} = 142.9$ Mpc), while the second uses the sound horizon from the best-fit ΛCDM model ($r_{\text{drag}} = 147.7$ Mpc). We observe in the right panel that the $n = 2$ model fits the properly calibrated BAO data points nearly as well as ΛCDM , while at the same time providing a much better fit to the SH0ES measurement.

As discussed in section 3.3, rolling scalar field models that inject energy in the period just prior to recombination require larger values of the scalar spectral index and amplitude of primordial fluctuations. This causes the late-time amplitude of matter fluctuations to be larger than their ΛCDM counterparts. This is potentially problematic since several measurements of the quantity $S_8 \equiv \sigma_8 \sqrt{\Omega_{\text{m}}/0.3}$ have returned slightly lower values than the ΛCDM expectation based on its CMB fit. We illustrate in figure 9 the joint marginalized posterior of S_8 and H_0 for both the $n = 2$ and N_{eff} models. Since the

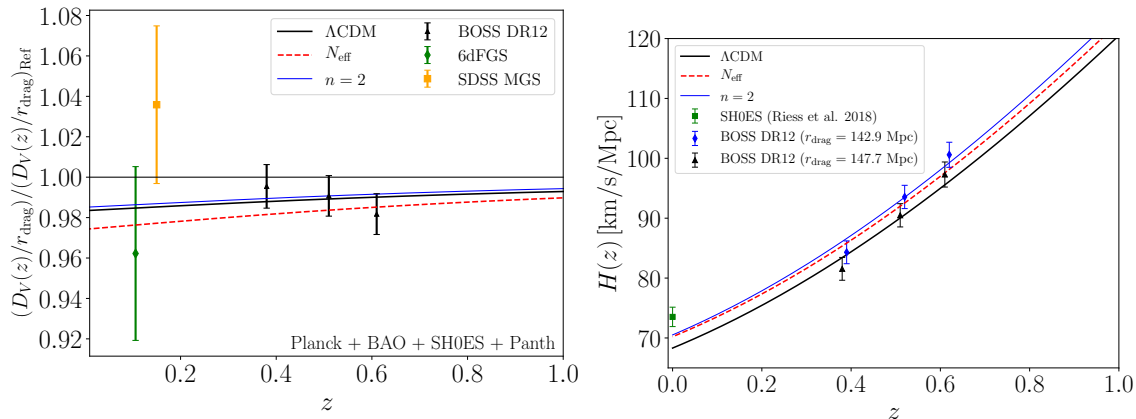


Figure 8. *Left panel:* The BAO distance ladder as expressed through the ratio $D_V(z)/r_{\text{drag}}$ normalized to the best-fit “Planck + BAO + Pantheon” Λ CDM reference model. *Right panel:* Hubble expansion history for $z < 1$. We show the H_0 measurement from ref. [5], as well as two sets of line-of-sight BOSS DR12 BAO measurements [148]: one calibrated to the sound horizon of the best-fit Λ CDM model (black triangles), and the other calibrated to that of the best-fit $n = 2$ model (blue diamonds). All curves shown in this figure are best-fit models to the data combination “Planck + BAO + SH0ES + Pantheon”.

$n = 2$ scalar field model has slightly larger values of both σ_8 and Ω_m as compared to N_{eff} , we find that it worsens the tension with the value of S_8 measured from weak lensing observations (e.g. ref. [156]). We note however that the robustness of this S_8 tension is still debated (see e.g. refs. [159, 160]) and more work is necessary to establish whether this is a problem for the kind of models considered here.

Another possible issue with these scalar field models is that the larger values of the Hubble constant is correlated with a larger reionization optical depth τ_{reio} , as can be seen in figure 6. Such large values of τ_{reio} could require new high-redshift sources in order to reionize the Universe at a higher redshift [161]. More recent analyses (see e.g. ref. [104]) have found lower values of τ_{reio} than we find here, although they are somewhat still larger than in Λ CDM.

Up to now, we have considered pure monomial potentials, $V \propto \phi^{2n}$, in which the more relevant ϕ^{2k} terms with $k < n$ have been set to zero. In realistic UV completions, however, one expects that these terms would be present at some order, and their absence would then reflect some degree of tuning in the model. For a sufficiently small mass term, the dominant effect is that the residual energy density in the scalar field comes to behave like an additional dark matter component once the scalar field amplitude has decayed such that $\langle m^2 \phi^2 \rangle \sim \rho_\phi$. At larger amplitudes, the field behaves as described in section 2. This additional dark matter slightly modifies the distance-redshift relationship, in particular decreasing the distance to the surface of last scattering. As long as the dark matter energy density is increased by less than one part in $\mathcal{O}(10^{-3})$, the effects are within our stated error bars and the above results will hold. For our best fit $n = 2$ model, this corresponds to a mass below $\sim 10^{-4} \text{eV}^4 / M_{\text{pl}}^2$, representing at most a 1% tuning given the size of the quartic coupling. We have neglected to include such a term for simplicity, and including it could actually improve the fit. While the best fit model has more dark matter than is found in Λ CDM, the increase in H_0 causes Ω_m to be slightly smaller, representing an increase in the redshift of dark energy domination. Including a small amount of additional dark matter in the late universe relative to its abundance near matter-radiation equality would then improve the fit to low- z BAO and supernovae data, at the cost of an increase

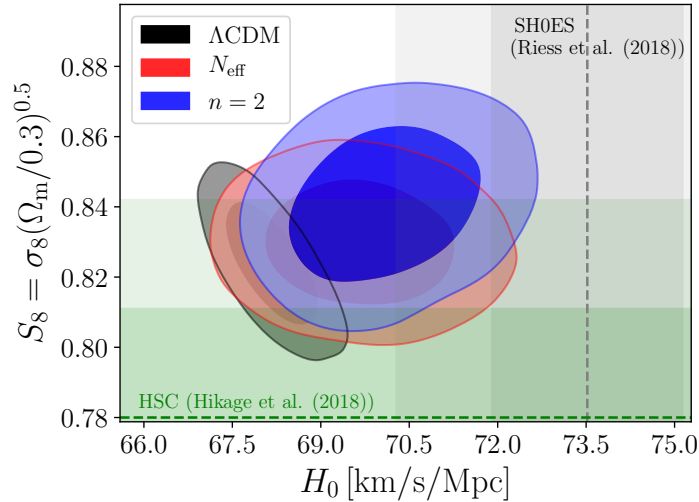


Figure 9. Marginalized posterior distributions in the S_8 - H_0 plane obtained using the data combination “Planck + BAO + SH0ES + Pantheon”. The gray vertical band shows the local Hubble constant measurement from ref. [5], while the horizontal green band shows the S_8 measurement from ref. [156].

in the required numerical precision to track the rapid field oscillations. We leave a detailed study to future work.

5 Conclusions

We see that scalar fields are good candidates for localized energy injection in the early universe that can in principle produce better combined fits to the CMB, BAO, and SH0ES than, *e.g.*, N_{eff} . We have considered models in which the scalar field spends a long time, spends a long time, spends a long lonely, lonely, lonely, lonely, lonely time frozen before beginning to roll near matter-radiation equality. In addition:

- We have classified the scalar field solutions for ϕ^{2n} potentials and highlighted a class of rolling solutions whose equation of state asymptotes to a constant value.
- Oscillating solutions exist only for $n \leq 3$ in a matter-dominated universe.
- A coarse-grained description of the evolution of the scalar field is insufficient to accurately describe the cosmological evolution near the maximum of the energy injection.
- These models predict larger values of σ_8 . Improvements in this measurement as well as other, more direct measurements of the matter power spectrum will help test these solutions in the future. We expect these models to be distinguishable at large k .
- A weakness of the model as it stands is the requirement that thawing occurs very close to matter-radiation equality at $T \sim \text{eV}$. A more complete model would also explain this, presumably through a triggering of the onset of rolling by the change in the background evolution (see *e.g.* refs. [75, 162, 163]).

- Our analysis requires a modest tuning. A small mass term which does not affect the physics around the energy injection might improve the fit to low- z BAO data. It might also be interesting to search for models in which the absence of a mass term is natural.
- In 2019, N_{eff} might still be a more compelling model since there is neither fine tuning nor a coincidence problem. However, if future measurements of the Hubble parameter have smaller error bars with the same central value, scalar field models could become favored as they allow larger values for H_0 .

Clearly the Hubble tension is one of the most intriguing discrepancies in cosmology today. Improved measurements of the CMB, $H(z)$, BAO at various redshifts, and the matter power spectrum (at both σ_8 and higher k), will ultimately give us greater insight into the existence of physics beyond Λ CDM.

Acknowledgments

We thank Daniel Grin, Julian Muñoz, Mustafa Amin, Manuel Buen-Abad, Martin Schmaltz, Daniel Eisenstein, and Vivian Poulin for useful discussions. L.R. wishes to thank Adam Riess for drawing our attention to ref. [64] and Matthias Steinmetz for an invitation to the symposium “The Hubble constant controversy: Status, implications, and solutions”, which inspired this work. D.P. wishes to thank Boston University for hospitality during completion of this work. We thank the Institut Henri Poincaré, where part of this work was carried out, for their hospitality. F.-Y. C.-R. and D.P. acknowledge the support of the National Aeronautical and Space Administration (NASA) ATP grant NNX16AI12G at Harvard University. D.P. is also supported by DOE grants DE-SC-0013607 and DE-SC-0010010. L.R. is supported by NSF grant PHY-1620806, the Kavli Foundation grant “Kavli Dream Team,” the Simons Fellows Program, the Guggenheim Foundation, and an IHES CARMIN fellowship. The work of PA is supported by the NSF grants PHY-0855591 and PHY-1216270. PA thanks the Galileo Galilei Institute for Theoretical Physics for their hospitality and the INFN for partial support during the completion of this work. The computations in this paper were run on the Odyssey cluster supported by the FAS Division of Science, Research Computing Group at Harvard University.

A Large Backreaction

The rolling solutions we have emphasized in section 2.1 may be somewhat surprising, given intuition derived from scalar fields evolving in non-expanding backgrounds. In the $M_{\text{pl}} \rightarrow \infty$ limit, there is no Hubble friction to damp oscillations, and so the rolling solutions do not exist. Furthermore, familiar examples of cosmological scalar fields often display oscillatory behavior even when initially over-damped by Hubble friction, such as the inflaton at the end of inflation. In this appendix we generalize the results of the main paper, which were derived working to zeroth order in the gravitational back-reaction, to the case where the scalar field dominates the energy density of the universe.

In this case ϕ^{2n} potentials have oscillating solutions for all values of $n > 0$. We can check self-consistency of these oscillatory solutions. If we assume an oscillatory solution, then the total energy density has equation of state w_{osc} , so we can use the Emden-Fowler analysis above with the identification $w_b = w_{\text{osc}}$. This implies that for

$$n < \frac{2}{1 - w_{\text{osc}}}, \quad \rho_{\text{total}} = \rho_{\phi}, \quad (\text{A.1})$$

only oscillatory solutions exist, which is always true since $w_{\text{osc}} = (n - 1)/(n + 1)$.

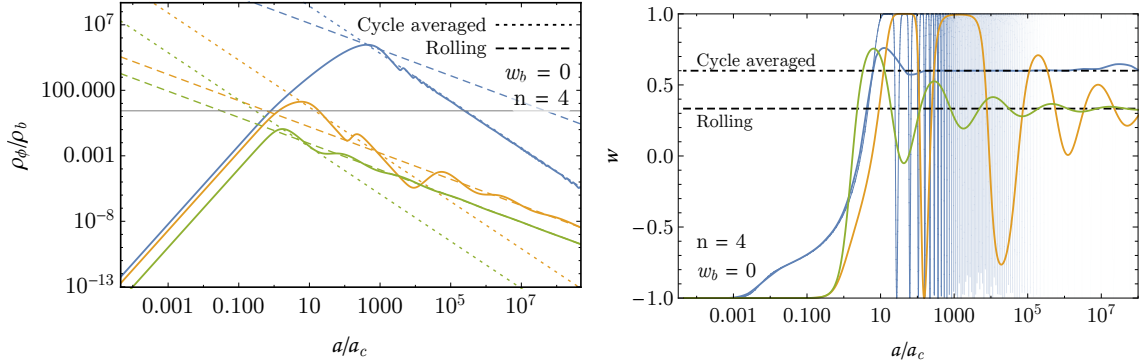


Figure 10. Evolution of the energy density (left) and the equation of state of the scalar field (right) as a function of the scale factor. Here, we compare the cases where the scalar field eventually dominates the energy density of the universe (blue and orange solid lines), with that in which it is always subdominant (solid green). The potential was chosen to be $V \propto \phi^{2n}$ with $n = 4$.

We show an example of such a solution for $n = 4$ in figure 10, where we take a toy matter-dominated cosmology (with $w_b = 0$). Here the Hubble constant is determined consistently including both the ρ_b and ρ_ϕ contributions. Note that this behavior is not used for our main results, since the fit to CMB data requires that the scalar field energy density is always subdominant.

We display three different choices of initial condition for the scalar field, corresponding to increasing peak energy fractions. Along the curve in green, the scalar field energy density is always subdominant to the background energy density, and the curve quickly asymptotes to the equation of state derived in section 2.1 for rolling solution with $w_\phi = 1/3$. Increasing the peak energy density beyond ρ_b , the solution becomes oscillatory, with a cycle-averaged equation of state given by w_{osc} , as demonstrated by the blue and orange curves. Eventually, the scalar field energy density redshifts enough that it becomes subdominant once again, and the field recovers the rolling solution. This is apparent along the orange curve, which is notably kinked near $a/a_c \sim 10^5$. It is interesting to note that this transition does not take place immediately, but rather long after the scalar field has become subdominant to the background.

B Beyond monomial potentials

The asymptotic behavior of scalar fields studied in section 2 is not unique to the monomial potentials considered there. Indeed, any potential which asymptotes to the monomial potential at small field values will exhibit the same asymptotic behavior. In this section we compare our results with the early dark energy fluid model of Ref. [64]. This fluid model aims to approximate [48] a scalar field evolving on a cosine potential, $V \propto (1 - \cos(\phi/f))^n$, which we also consider here. Of course when $\phi \ll f$, this is well approximated by $V \sim \phi^{2n}$.

We want to disentangle two possible explanations for differences between our results and those of Ref. [64]. First, the shape of the potential ϕ^{2n} is different from the $(1 - \cos(\phi/f))^n$ at large field values. Second, the smooth fluid approximation considered in Ref. [64] fails to capture the dynamics of an oscillating scalar field near the peak of the energy injection. We present a few examples to make these distinctions concrete.

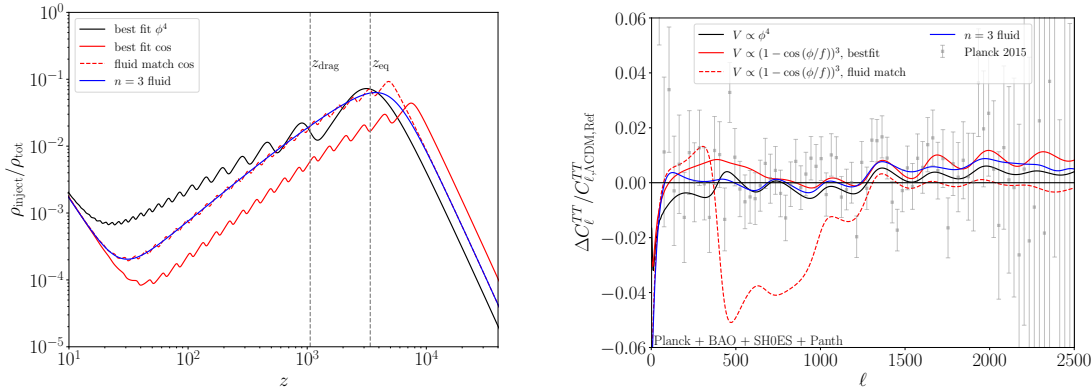


Figure 11. Energy injection profile (left) and CMB temperature residuals (right) for 4 different models. Here, we compare two different cosine potentials and a fluid model with our best fit ϕ^4 model.

To select benchmarks, we pick the best fit case within our models, $n = 2$ ($V \propto \phi^4$) and that of the fluid models in Ref. [64], for which $n = 3$. We label this the “n=3 fluid” model in figure 11. For comparison, we show results for a cosine model. As the fluid model was designed to reproduce the results of the cosine, we fix $n = 3$ for the cosine as well.

The remaining parameters in the cosine model are the coefficient of the potential, the initial field value, and the field range f . Two of these parameters control the height and the redshift of the maximum energy injection, similar to the case of the monomial potential. The remaining parameter, which we take to be f , is undetermined. In particular it is not clear which value of f corresponds to the best fit fluid model. For figure 11 we fix $f = 0.05M_{\text{Pl}}$.

Fixing the height and redshift of energy injection relates the initial field value with f . For $f \simeq M_{\text{Pl}}$ the initial field value required to get the best fit injection shape is much smaller than f , so that the cosine potential reduces to the monomial potential studied in the previous section. As f is reduced, the required initial field approaches πf , so that small values of f require a fine-tuned initial condition. Furthermore, for $\phi_i \gtrsim f$, $V''(\phi_i) < 0$ corresponding to an instability in the spectrum of fluctuations. For $f \lesssim 0.01M_{\text{Pl}}$, the instability causes the fluctuations to grow so rapidly that linear perturbation theory becomes invalid. For our choice of $f = 0.05M_{\text{Pl}}$ the fluctuations remain under control, but the initial field value must be tuned at the $\mathcal{O}(1\%)$ level.

In figure 11 we show two choices for the cosine potential. The “fluid match cos” model (shown in dashed red) is chosen to match the background energy injection shape of the best fit fluid model as closely as possible. The remaining cosmological parameters were taken from the best fit values in [64]. We also present the “best fit cos” model (shown in solid red) in which all parameters are freely floated, but does not correspond to the best fit fluid model in any way. In the fluid case we use the public code developed by [164] to implement the fluctuations. For the ϕ^4 and cosine potentials we use the equations of motion of the scalar field to derive the cosmological evolution of fluctuations.

We show our results for background cosmology in each of the cases described above in figure 11. We see that at the background level the “fluid match cos” model does follow the best fit fluid model at late times. However, it is significantly different at the peak of the energy injection. The “best fit cos” model has a much lower peak injection energy than all the other models, reflecting the relative inability of the CMB to accommodate large energy injections of this form. In particular, the energy injection in the “best fit cos” model does not resemble that of the fluid model at all. We plot the

residuals of the temperature power spectrum with respect to a reference Λ CDM model. The models that were fit to the CMB, i.e. ϕ^4 , “best fit cos” and the “best fit fluid” model all have small residuals (as expected from the fact that these models were chosen by minimizing CMB likelihoods). However, the “fluid match cos” model has enormous residuals in a range of ℓ corresponding to modes which enter the horizon around the peak of the energy injection. This is quite consistent with our argument above: at the onset of oscillations, the fluid model is in no way an approximation to the cos potential.

Finally, an interesting question is if there is *any* model that does reproduce the fluid model. Even if one did reproduce the smooth energy injection of the fluid model, it is not clear at all that the fluctuations in that particular model have the same sound speed as the fluid model. In particular, we can (numerically) derive a potential for a scalar field such that the energy injection is identical to the fluid model. However, this potential has a region for which $V''(\phi) < 0$, and so the fluctuations in this region are unstable. It would seem that it is an open question whether the fluid model can ever be realized in a realistic physics model.

References

- [1] A. G. Riess, L. Macri, S. Casertano, H. Lampeitl, H. C. Ferguson, A. V. Filippenko, S. W. Jha, W. Li, and R. Chornock, “A 3% Solution: Determination of the Hubble Constant with the Hubble Space Telescope and Wide Field Camera 3,” *Astrophys. J.* **730** (Apr., 2011) 119, [arXiv:1103.2976](#).
- [2] W. L. Freedman, B. F. Madore, V. Scowcroft, C. Burns, A. Monson, S. E. Persson, M. Seibert, and J. Rigby, “Carnegie Hubble Program: A Mid-infrared Calibration of the Hubble Constant,” *Astrophys. J.* **758** no. 1, (Oct., 2012) 24, [arXiv:1208.3281](#) [[astro-ph.CO](#)].
- [3] A. G. Riess *et al.*, “A 2.4% Determination of the Local Value of the Hubble Constant,” *Astrophys. J.* **826** no. 1, (2016) 56, [arXiv:1604.01424](#) [[astro-ph.CO](#)].
- [4] S. H. Suyu *et al.*, “H0LiCOW – I. H0 Lenses in COSMOGRAIL’s Wellspring: program overview,” *Mon. Not. Roy. Astron. Soc.* **468** no. 3, (2017) 2590–2604, [arXiv:1607.00017](#) [[astro-ph.CO](#)].
- [5] A. G. Riess *et al.*, “Milky Way Cepheid Standards for Measuring Cosmic Distances and Application to Gaia DR2: Implications for the Hubble Constant,” *Astrophys. J.* **861** no. 2, (2018) 126, [arXiv:1804.10655](#) [[astro-ph.CO](#)].
- [6] V. Bonvin *et al.*, “H0LiCOW – V. New COSMOGRAIL time delays of HE 0435-1223: H_0 to 3.8 per cent precision from strong lensing in a flat Λ CDM model,” *Mon. Not. Roy. Astron. Soc.* **465** no. 4, (2017) 4914–4930, [arXiv:1607.01790](#) [[astro-ph.CO](#)].
- [7] S. Dhawan, S. W. Jha, and B. Leibundgut, “Measuring the Hubble constant with Type Ia supernovae as near-infrared standard candles,” *Astron. Astrophys.* **609** (2018) A72, [arXiv:1707.00715](#) [[astro-ph.CO](#)].
- [8] S. Birrer, T. Treu, C. E. Rusu, V. Bonvin, C. D. Fassnacht, J. H. H. Chan, A. Agnello, A. J. Shajib, G. C. F. Chen, M. Auger, F. Courbin, S. Hilbert, D. Sluse, S. H. Suyu, K. C. Wong, P. Marshall, B. C. Lemaux, and G. Meylan, “H0LiCOW - IX. Cosmographic analysis of the doubly imaged quasar SDSS 1206+4332 and a new measurement of the Hubble constant,” *Mon. Not. R. Astron. Soc.* **484** (Apr, 2019) 4726–4753, [arXiv:1809.01274](#) [[astro-ph.CO](#)].
- [9] **DES, LIGO Scientific, Virgo** Collaboration, M. Soares-Santos *et al.*, “First Measurement of the Hubble Constant from a Dark Standard Siren using the Dark Energy Survey Galaxies and the LIGO/Virgo Binary–Black-hole Merger GW170814,” *Astrophys. J. Lett.* **876** no. 1, (2019) L7, [arXiv:1901.01540](#) [[astro-ph.CO](#)].

- [10] A. G. Riess, S. Casertano, W. Yuan, L. M. Macri, and D. Scolnic, “Large Magellanic Cloud Cepheid Standards Provide a 1% Foundation for the Determination of the Hubble Constant and Stronger Evidence for Physics beyond Λ CDM,” *Astrophys. J.* **876** no. 1, (2019) 85, [arXiv:1903.07603 \[astro-ph.CO\]](#).
- [11] K. C. Wong *et al.*, “H0LiCOW – XIII. A 2.4 per cent measurement of H0 from lensed quasars: 5.3σ tension between early- and late-Universe probes,” *Mon. Not. Roy. Astron. Soc.* **498** no. 1, (2020) 1420–1439, [arXiv:1907.04869 \[astro-ph.CO\]](#).
- [12] C. D. Huang, A. G. Riess, W. Yuan, L. M. Macri, N. L. Zakamska, S. Casertano, P. A. Whitelock, S. L. Hoffmann, A. V. Filippenko, and D. Scolnic, “Hubble Space Telescope Observations of Mira Variables in the Type Ia Supernova Host NGC 1559: An Alternative Candle to Measure the Hubble Constant,” [arXiv:1908.10883 \[astro-ph.CO\]](#).
- [13] E. Kourkchi, R. B. Tully, G. S. Anand, H. M. Courtois, A. Dupuy, J. D. Neill, L. Rizzi, and M. Seibert, “Cosmicflows-4: The Calibration of Optical and Infrared Tully–Fisher Relations,” *Astrophys. J.* **896** no. 1, (2020) 3, [arXiv:2004.14499 \[astro-ph.GA\]](#).
- [14] M. J. Reid, D. W. Pesce, and A. G. Riess, “An Improved Distance to NGC 4258 and its Implications for the Hubble Constant,” *Astrophys. J. Lett.* **886** no. 2, (2019) L27, [arXiv:1908.05625 \[astro-ph.GA\]](#).
- [15] W. L. Freedman, B. F. Madore, D. Hatt, T. J. Hoyt, I. S. Jang, R. L. Beaton, C. R. Burns, M. G. Lee, A. J. Monson, J. R. Neeley, M. M. Phillips, J. A. Rich, and M. Seibert, “The Carnegie-Chicago Hubble Program. VIII. An Independent Determination of the Hubble Constant Based on the Tip of the Red Giant Branch,” *Astrophys. J.* **882** no. 1, (Sept., 2019) 34, [arXiv:1907.05922 \[astro-ph.CO\]](#).
- [16] W. L. Freedman, B. F. Madore, T. Hoyt, I. S. Jang, R. Beaton, M. G. Lee, A. Monson, J. Neeley, and J. Rich, “Calibration of the Tip of the Red Giant Branch,” *Astrophys. J.* **891** no. 1, (Mar., 2020) 57, [arXiv:2002.01550 \[astro-ph.GA\]](#).
- [17] D. W. Pesce *et al.*, “The Megamaser Cosmology Project. XIII. Combined Hubble constant constraints,” *Astrophys. J. Lett.* **891** no. 1, (2020) L1, [arXiv:2001.09213 \[astro-ph.CO\]](#).
- [18] N. Khetan *et al.*, “A new measurement of the Hubble constant using Type Ia supernovae calibrated with surface brightness fluctuations,” *Astron. Astrophys.* **647** (2021) A72, [arXiv:2008.07754 \[astro-ph.CO\]](#).
- [19] J. P. Blakeslee, J. B. Jensen, C.-P. Ma, P. A. Milne, and J. E. Greene, “The Hubble Constant from Infrared Surface Brightness Fluctuation Distances,” *Astrophys. J.* **911** no. 1, (2021) 65, [arXiv:2101.02221 \[astro-ph.CO\]](#).
- [20] S. Birrer *et al.*, “TDCOSMO - IV. Hierarchical time-delay cosmography – joint inference of the Hubble constant and galaxy density profiles,” *Astron. Astrophys.* **643** (2020) A165, [arXiv:2007.02941 \[astro-ph.CO\]](#).
- [21] A. G. Riess *et al.*, “A Comprehensive Measurement of the Local Value of the Hubble Constant with 1 $\text{km s}^{-1} \text{Mpc}^{-1}$ Uncertainty from the Hubble Space Telescope and the SH0ES Team,” *Astrophys. J. Lett.* **934** no. 1, (2022) L7, [arXiv:2112.04510 \[astro-ph.CO\]](#).
- [22] W. L. Freedman, “Measurements of the Hubble Constant: Tensions in Perspective,” *Astrophys. J.* **919** no. 1, (2021) 16, [arXiv:2106.15656 \[astro-ph.CO\]](#).
- [23] **WMAP** Collaboration, G. Hinshaw *et al.*, “Nine-Year Wilkinson Microwave Anisotropy Probe (WMAP) Observations: Cosmological Parameter Results,” *Astrophys. J. Suppl.* **208** (2013) 19, [arXiv:1212.5226 \[astro-ph.CO\]](#).

- [24] Planck Collaboration, Ade, P. A. R., *et al.*, “Planck 2015 results xiii. cosmological parameters,” *A&A* **594** (2016) A13. <http://dx.doi.org/10.1051/0004-6361/201525830>.
- [25] **Planck** Collaboration, N. Aghanim *et al.*, “Planck 2018 results. VI. Cosmological parameters,” [arXiv:1807.06209](https://arxiv.org/abs/1807.06209) [[astro-ph.CO](https://arxiv.org/abs/1807.06209)].
- [26] **HST** Collaboration, W. L. Freedman *et al.*, “Final results from the Hubble Space Telescope key project to measure the Hubble constant,” *Astrophys. J.* **553** (2001) 47–72, [arXiv:astro-ph/0012376](https://arxiv.org/abs/astro-ph/0012376) [[astro-ph](https://arxiv.org/abs/astro-ph/0012376)].
- [27] L. Verde, T. Treu, and A. G. Riess, “Tensions between the Early and the Late Universe,” *Nature Astron.* **3** (7, 2019) 891, [arXiv:1907.10625](https://arxiv.org/abs/1907.10625) [[astro-ph.CO](https://arxiv.org/abs/1907.10625)].
- [28] E. Di Valentino, O. Mena, S. Pan, L. Visinelli, W. Yang, A. Melchiorri, D. F. Mota, A. G. Riess, and J. Silk, “In the realm of the Hubble tension—a review of solutions,” *Class. Quant. Grav.* **38** no. 15, (2021) 153001, [arXiv:2103.01183](https://arxiv.org/abs/2103.01183) [[astro-ph.CO](https://arxiv.org/abs/2103.01183)].
- [29] L. Perivolaropoulos and F. Skara, “Challenges for Λ CDM: An update,” *New Astron. Rev.* **95** (2022) 101659, [arXiv:2105.05208](https://arxiv.org/abs/2105.05208) [[astro-ph.CO](https://arxiv.org/abs/2105.05208)].
- [30] E. Abdalla *et al.*, “Cosmology intertwined: A review of the particle physics, astrophysics, and cosmology associated with the cosmological tensions and anomalies,” *JHEAp* **34** (2022) 49–211, [arXiv:2203.06142](https://arxiv.org/abs/2203.06142) [[astro-ph.CO](https://arxiv.org/abs/2203.06142)].
- [31] **Nearby Supernova factory** Collaboration, M. Rigault *et al.*, “Evidence of Environmental Dependencies of Type Ia Supernovae from the Nearby Supernova Factory indicated by Local $H\alpha$,” *Astron. Astrophys.* **560** (2013) A66, [arXiv:1309.1182](https://arxiv.org/abs/1309.1182) [[astro-ph.CO](https://arxiv.org/abs/1309.1182)]. [Corrigendum: *Astron. Astrophys.*612,C1(2018)].
- [32] **Nearby Supernova Factory** Collaboration, M. Rigault *et al.*, “Strong Dependence of Type Ia Supernova Standardization on the Local Specific Star Formation Rate,” *Astron. Astrophys.* **644** (2020) A176, [arXiv:1806.03849](https://arxiv.org/abs/1806.03849) [[astro-ph.CO](https://arxiv.org/abs/1806.03849)].
- [33] D. O. Jones *et al.*, “Should Type Ia Supernova Distances be Corrected for their Local Environments?,” *Astrophys. J.* **867** no. 2, (2018) 108, [arXiv:1805.05911](https://arxiv.org/abs/1805.05911) [[astro-ph.CO](https://arxiv.org/abs/1805.05911)].
- [34] T. Shanks, L. Hogarth, and N. Metcalfe, “GAIA Cepheid parallaxes and ‘Local Hole’ relieve H_0 tension,” *Mon. Not. Roy. Astron. Soc.* **484** (2019) L64, [arXiv:1810.02595](https://arxiv.org/abs/1810.02595) [[astro-ph.CO](https://arxiv.org/abs/1810.02595)].
- [35] A. G. Riess, S. Casertano, D. Kenworthy, D. Scolnic, and L. Macri, “Seven Problems with the Claims Related to the Hubble Tension in [arXiv:1810.02595](https://arxiv.org/abs/1810.02595),” [arXiv:1810.03526](https://arxiv.org/abs/1810.03526) [[astro-ph.CO](https://arxiv.org/abs/1810.03526)].
- [36] W. D. Kenworthy, D. Scolnic, and A. Riess, “The Local Perspective on the Hubble Tension: Local Structure Does Not Impact Measurement of the Hubble Constant,” *Astrophys. J.* **875** no. 2, (2019) 145, [arXiv:1901.08681](https://arxiv.org/abs/1901.08681) [[astro-ph.CO](https://arxiv.org/abs/1901.08681)].
- [37] G. Efstathiou, “A Lockdown Perspective on the Hubble Tension (with comments from the SHOES team),” [arXiv:2007.10716](https://arxiv.org/abs/2007.10716) [[astro-ph.CO](https://arxiv.org/abs/2007.10716)].
- [38] E. Mortsell, A. Goobar, J. Johansson, and S. Dhawan, “Sensitivity of the Hubble Constant Determination to Cepheid Calibration,” *Astrophys. J.* **933** no. 2, (2022) 212, [arXiv:2105.11461](https://arxiv.org/abs/2105.11461) [[astro-ph.CO](https://arxiv.org/abs/2105.11461)].
- [39] E. Mortsell, A. Goobar, J. Johansson, and S. Dhawan, “The Hubble Tension Revisited: Additional Local Distance Ladder Uncertainties,” *Astrophys. J.* **935** no. 1, (2022) 58, [arXiv:2106.09400](https://arxiv.org/abs/2106.09400) [[astro-ph.CO](https://arxiv.org/abs/2106.09400)].
- [40] J. Evslin, A. A. Sen, and Ruchika, “Price of shifting the Hubble constant,” *Phys. Rev.* **D97** no. 10, (2018) 103511, [arXiv:1711.01051](https://arxiv.org/abs/1711.01051) [[astro-ph.CO](https://arxiv.org/abs/1711.01051)].

- [41] K. Aylor, M. Joy, L. Knox, M. Millea, S. Raghunathan, and W. L. Kimmy Wu, “Sounds Discordant: Classical Distance Ladder and Λ CDM-based Determinations of the Cosmological Sound Horizon,” *Astrophys. J.* **874** (Mar, 2019) 4, [arXiv:1811.00537 \[astro-ph.CO\]](#).
- [42] L. Knox and M. Millea, “Hubble constant hunter’s guide,” *Phys. Rev. D* **101** (Feb, 2020) 043533.
- [43] K. Jedamzik and L. Pogosian, “Relieving the Hubble tension with primordial magnetic fields,” *Phys. Rev. Lett.* **125** no. 18, (2020) 181302, [arXiv:2004.09487 \[astro-ph.CO\]](#).
- [44] C.-T. Chiang and A. Slosar, “Inferences of H_0 in presence of a non-standard recombination,” [arXiv:1811.03624 \[astro-ph.CO\]](#).
- [45] L. Hart and J. Chluba, “Updated fundamental constant constraints from Planck 2018 data and possible relations to the Hubble tension,” *Mon. Not. Roy. Astron. Soc.* **493** no. 3, (2020) 3255–3263, [arXiv:1912.03986 \[astro-ph.CO\]](#).
- [46] T. Sekiguchi and T. Takahashi, “Early recombination as a solution to the H_0 tension,” *Phys. Rev. D* **103** no. 8, (2021) 083507, [arXiv:2007.03381 \[astro-ph.CO\]](#).
- [47] A. Hojjati, E. V. Linder, and J. Samsing, “New Constraints on the Early Expansion History of the Universe,” *Phys. Rev. Lett.* **111** no. 4, (2013) 041301, [arXiv:1304.3724 \[astro-ph.CO\]](#).
- [48] V. Poulin, T. L. Smith, D. Grin, T. Karwal, and M. Kamionkowski, “Cosmological implications of ultralight axionlike fields,” *Phys. Rev.* **D98** no. 8, (2018) 083525, [arXiv:1806.10608 \[astro-ph.CO\]](#).
- [49] E. Di Valentino, E. V. Linder, and A. Melchiorri, “Vacuum phase transition solves the H_0 tension,” *Phys. Rev.* **D97** no. 4, (2018) 043528, [arXiv:1710.02153 \[astro-ph.CO\]](#).
- [50] F. D’Eramo, R. Z. Ferreira, A. Notari, and J. L. Bernal, “Hot Axions and the H_0 tension,” *JCAP* **1811** no. 11, (2018) 014, [arXiv:1808.07430 \[hep-ph\]](#).
- [51] V. Poulin, K. K. Boddy, S. Bird, and M. Kamionkowski, “Implications of an extended dark energy cosmology with massive neutrinos for cosmological tensions,” *Phys. Rev.* **D97** no. 12, (2018) 123504, [arXiv:1803.02474 \[astro-ph.CO\]](#).
- [52] K. L. Pandey, T. Karwal, and S. Das, “Alleviating the H_0 and σ_8 anomalies with a decaying dark matter model,” *JCAP* **07** (2020) 026, [arXiv:1902.10636 \[astro-ph.CO\]](#).
- [53] E. Mörtzell and S. Dhawan, “Does the Hubble constant tension call for new physics?,” *JCAP* **1809** no. 09, (2018) 025, [arXiv:1801.07260 \[astro-ph.CO\]](#).
- [54] K. Vattis, S. M. Koushiappas, and A. Loeb, “Dark matter decaying in the late Universe can relieve the H_0 tension,” *Phys. Rev. D* **99** no. 12, (2019) 121302, [arXiv:1903.06220 \[astro-ph.CO\]](#).
- [55] J. Renk, M. Zumalacárregui, F. Montanari, and A. Barreira, “Galileon gravity in light of ISW, CMB, BAO and H_0 data,” *JCAP* **1710** no. 10, (2017) 020, [arXiv:1707.02263 \[astro-ph.CO\]](#).
- [56] N. Khosravi, S. Baghran, N. Afshordi, and N. Altamirano, “ \ddot{u} Λ CDM: H_0 tension as a hint for Über-Gravity,” [arXiv:1710.09366 \[astro-ph.CO\]](#).
- [57] W. Yang, A. Mukherjee, E. Di Valentino, and S. Pan, “Interacting dark energy with time varying equation of state and the H_0 tension,” *Phys. Rev.* **D98** no. 12, (2018) 123527, [arXiv:1809.06883 \[astro-ph.CO\]](#).
- [58] W. Yang, S. Pan, E. Di Valentino, R. C. Nunes, S. Vagnozzi, and D. F. Mota, “Tale of stable interacting dark energy, observational signatures, and the H_0 tension,” *JCAP* **1809** no. 09, (2018) 019, [arXiv:1805.08252 \[astro-ph.CO\]](#).
- [59] W. Yang, S. Pan, E. Di Valentino, E. N. Saridakis, and S. Chakraborty, “Observational constraints on

- one-parameter dynamical dark-energy parametrizations and the H_0 tension,” *Phys. Rev.* **D99** no. 4, (2019) 043543, [arXiv:1810.05141 \[astro-ph.CO\]](#).
- [60] C. D. Kreisch, F.-Y. Cyr-Racine, and O. Doré, “Neutrino puzzle: Anomalies, interactions, and cosmological tensions,” *Phys. Rev. D* **101** no. 12, (2020) 123505, [arXiv:1902.00534 \[astro-ph.CO\]](#).
- [61] G. Benevento, W. Hu, and M. Raveri, “Can Late Dark Energy Transitions Raise the Hubble constant?,” *Phys. Rev. D* **101** no. 10, (2020) 103517, [arXiv:2002.11707 \[astro-ph.CO\]](#).
- [62] J. C. Hill and E. J. Baxter, “Can Early Dark Energy Explain EDGES?,” *JCAP* **08** (2018) 037, [arXiv:1803.07555 \[astro-ph.CO\]](#).
- [63] K. S. Karkare and S. Bird, “Constraining the Expansion History and Early Dark Energy with Line Intensity Mapping,” *Phys. Rev. D* **98** no. 4, (2018) 043529, [arXiv:1806.09625 \[astro-ph.CO\]](#).
- [64] V. Poulin, T. L. Smith, T. Karwal, and M. Kamionkowski, “Early Dark Energy Can Resolve The Hubble Tension,” *Phys. Rev. Lett.* **122** no. 22, (2019) 221301, [arXiv:1811.04083 \[astro-ph.CO\]](#).
- [65] F. Noble Chamings, A. Avgoustidis, E. J. Copeland, A. M. Green, and B. Li, “Early dark energy constraints on growing neutrino quintessence cosmologies,” *Phys. Rev. D* **100** no. 4, (2019) 043525, [arXiv:1904.00884 \[astro-ph.CO\]](#).
- [66] T. L. Smith, V. Poulin, and M. A. Amin, “Oscillating scalar fields and the Hubble tension: a resolution with novel signatures,” *Phys. Rev. D* **101** no. 6, (2020) 063523, [arXiv:1908.06995 \[astro-ph.CO\]](#).
- [67] A. Bhattacharyya and S. Pal, “Constraining Dark Energy Perturbations: the Role of Early Dark Energy,” [arXiv:1907.10946 \[astro-ph.CO\]](#).
- [68] M.-X. Lin, G. Benevento, W. Hu, and M. Raveri, “Acoustic Dark Energy: Potential Conversion of the Hubble Tension,” *Phys. Rev. D* **100** no. 6, (2019) 063542, [arXiv:1905.12618 \[astro-ph.CO\]](#).
- [69] M.-X. Lin, W. Hu, and M. Raveri, “Testing H_0 in Acoustic Dark Energy with Planck and ACT Polarization,” *Phys. Rev. D* **102** (2020) 123523, [arXiv:2009.08974 \[astro-ph.CO\]](#).
- [70] L. Yin, “Reducing the H_0 tension with exponential acoustic dark energy,” *Eur. Phys. J. C* **82** no. 1, (2022) 78, [arXiv:2012.13917 \[astro-ph.CO\]](#).
- [71] A. Chudaykin, D. Gorbunov, and N. Nedelko, “Combined analysis of Planck and SPTPol data favors the early dark energy models,” *JCAP* **08** (2020) 013, [arXiv:2004.13046 \[astro-ph.CO\]](#).
- [72] M. M. Ivanov, E. McDonough, J. C. Hill, M. Simonović, M. W. Toomey, S. Alexander, and M. Zaldarriaga, “Constraining Early Dark Energy with Large-Scale Structure,” *Phys. Rev. D* **102** no. 10, (2020) 103502, [arXiv:2006.11235 \[astro-ph.CO\]](#).
- [73] H. Khoraminezhad, M. Viel, C. Baccigalupi, and M. Archidiacono, “Constraints on the Spacetime Dynamics of an Early Dark Energy Component,” *JCAP* **07** (2020) 039, [arXiv:2001.10252 \[astro-ph.CO\]](#).
- [74] J. C. Hill, E. McDonough, M. W. Toomey, and S. Alexander, “Early dark energy does not restore cosmological concordance,” *Phys. Rev. D* **102** no. 4, (2020) 043507, [arXiv:2003.07355 \[astro-ph.CO\]](#).
- [75] J. Sakstein and M. Trodden, “Early Dark Energy from Massive Neutrinos as a Natural Resolution of the Hubble Tension,” *Phys. Rev. Lett.* **124** no. 16, (2020) 161301, [arXiv:1911.11760 \[astro-ph.CO\]](#).
- [76] A. Mandal and S. Nadkarni-Ghosh, “One-point probability distribution function from spherical collapse: early dark energy versus Λ CDM,” *Mon. Not. Roy. Astron. Soc.* **498** no. 1, (2020) 355–372, [arXiv:1910.14347 \[astro-ph.CO\]](#).

- [77] F. Niedermann and M. S. Sloth, “Resolving the Hubble tension with new early dark energy,” *Phys. Rev. D* **102** no. 6, (2020) 063527, [arXiv:2006.06686 \[astro-ph.CO\]](#).
- [78] G. Ye and Y.-S. Piao, “ T_0 censorship of early dark energy and AdS vacua,” *Phys. Rev. D* **102** no. 8, (2020) 083523, [arXiv:2008.10832 \[astro-ph.CO\]](#).
- [79] M. Braglia, W. T. Emond, F. Finelli, A. E. Gumrukcuoglu, and K. Koyama, “Unified framework for early dark energy from α -attractors,” *Phys. Rev. D* **102** no. 8, (2020) 083513, [arXiv:2005.14053 \[astro-ph.CO\]](#).
- [80] L. A. García, L. Castañeda, and J. M. Tejeiro, “A novel early Dark Energy model,” *New Astron.* **84** (2021) 101503, [arXiv:2009.07357 \[astro-ph.CO\]](#).
- [81] K. Freese and M. W. Winkler, “Chain early dark energy: A Proposal for solving the Hubble tension and explaining today’s dark energy,” *Phys. Rev. D* **104** no. 8, (2021) 083533, [arXiv:2102.13655 \[astro-ph.CO\]](#).
- [82] A. Klypin, V. Poulin, F. Prada, J. Primack, M. Kamionkowski, V. Avila-Reese, A. Rodriguez-Puebla, P. Behroozi, D. Hellinger, and T. L. Smith, “Clustering and Halo Abundances in Early Dark Energy Cosmological Models,” *Mon. Not. Roy. Astron. Soc.* **504** no. 1, (2021) 769–781, [arXiv:2006.14910 \[astro-ph.CO\]](#).
- [83] O. Seto and Y. Toda, “Comparing early dark energy and extra radiation solutions to the Hubble tension with BBN,” *Phys. Rev. D* **103** no. 12, (2021) 123501, [arXiv:2101.03740 \[astro-ph.CO\]](#).
- [84] Z. J. Weiner, P. Adshead, and J. T. Giblin, “Constraining early dark energy with gravitational waves before recombination,” *Phys. Rev. D* **103** no. 2, (2021) L021301, [arXiv:2008.01732 \[astro-ph.CO\]](#).
- [85] S. X. Tian and Z.-H. Zhu, “Early dark energy in k -essence,” *Phys. Rev. D* **103** no. 4, (2021) 043518, [arXiv:2102.06399 \[gr-qc\]](#).
- [86] A. Gómez-Valent, Z. Zheng, L. Amendola, V. Pettorino, and C. Wetterich, “Early dark energy in the pre- and postrecombination epochs,” *Phys. Rev. D* **104** no. 8, (2021) 083536, [arXiv:2107.11065 \[astro-ph.CO\]](#).
- [87] T. L. Smith, V. Poulin, J. L. Bernal, K. K. Boddy, M. Kamionkowski, and R. Murgia, “Early dark energy is not excluded by current large-scale structure data,” *Phys. Rev. D* **103** no. 12, (2021) 123542, [arXiv:2009.10740 \[astro-ph.CO\]](#).
- [88] R. Murgia, G. F. Abellán, and V. Poulin, “Early dark energy resolution to the Hubble tension in light of weak lensing surveys and lensing anomalies,” *Phys. Rev. D* **103** no. 6, (2021) 063502, [arXiv:2009.10733 \[astro-ph.CO\]](#).
- [89] A. Gogoi, R. K. Sharma, P. Chanda, and S. Das, “Early Mass-varying Neutrino Dark Energy: Nugget Formation and Hubble Anomaly,” *Astrophys. J.* **915** no. 2, (2021) 132, [arXiv:2005.11889 \[astro-ph.CO\]](#).
- [90] A. Chudaykin, D. Gorbunov, and N. Nedelko, “Exploring an early dark energy solution to the Hubble tension with Planck and SPTPol data,” *Phys. Rev. D* **103** no. 4, (2021) 043529, [arXiv:2011.04682 \[astro-ph.CO\]](#).
- [91] S. Nojiri, S. D. Odintsov, D. Saez-Chillon Gomez, and G. S. Sharov, “Modeling and testing the equation of state for (Early) dark energy,” *Phys. Dark Univ.* **32** (2021) 100837, [arXiv:2103.05304 \[gr-qc\]](#).
- [92] M. Carrillo González, Q. Liang, J. Sakstein, and M. Trodden, “Neutrino-Assisted Early Dark Energy: Theory and Cosmology,” *JCAP* **04** (2021) 063, [arXiv:2011.09895 \[astro-ph.CO\]](#).

- [93] F. Niedermann and M. S. Sloth, “New early dark energy,” *Phys. Rev. D* **103** no. 4, (2021) L041303, [arXiv:1910.10739 \[astro-ph.CO\]](#).
- [94] F. Niedermann and M. S. Sloth, “New Early Dark Energy is compatible with current LSS data,” *Phys. Rev. D* **103** no. 10, (2021) 103537, [arXiv:2009.00006 \[astro-ph.CO\]](#).
- [95] J.-Q. Jiang and Y.-S. Piao, “Testing AdS early dark energy with Planck, SPTpol, and LSS data,” *Phys. Rev. D* **104** no. 10, (2021) 103524, [arXiv:2107.07128 \[astro-ph.CO\]](#).
- [96] G. Ye, J. Zhang, and Y.-S. Piao, “Resolving both H_0 and S_8 tensions with AdS early dark energy and ultralight axion,” [arXiv:2107.13391 \[astro-ph.CO\]](#).
- [97] J. C. Hill *et al.*, “Atacama Cosmology Telescope: Constraints on prerecombination early dark energy,” *Phys. Rev. D* **105** no. 12, (2022) 123536, [arXiv:2109.04451 \[astro-ph.CO\]](#).
- [98] T. Karwal, M. Raveri, B. Jain, J. Khoury, and M. Trodden, “Chameleon early dark energy and the Hubble tension,” *Phys. Rev. D* **105** no. 6, (2022) 063535, [arXiv:2106.13290 \[astro-ph.CO\]](#).
- [99] E. McDonough, M.-X. Lin, J. C. Hill, W. Hu, and S. Zhou, “Early dark sector, the Hubble tension, and the swampland,” *Phys. Rev. D* **106** no. 4, (2022) 043525, [arXiv:2112.09128 \[astro-ph.CO\]](#).
- [100] A. La Posta, T. Louis, X. Garrido, and J. C. Hill, “Constraints on prerecombination early dark energy from SPT-3G public data,” *Phys. Rev. D* **105** no. 8, (2022) 083519, [arXiv:2112.10754 \[astro-ph.CO\]](#).
- [101] A. Gómez-Valent, Z. Zheng, L. Amendola, C. Wetterich, and V. Pettorino, “Coupled and uncoupled early dark energy, massive neutrinos, and the cosmological tensions,” *Phys. Rev. D* **106** no. 10, (2022) 103522, [arXiv:2207.14487 \[astro-ph.CO\]](#).
- [102] K. Kojima and Y. Okubo, “Early dark energy from a higher-dimensional gauge theory,” *Phys. Rev. D* **106** no. 6, (2022) 063540, [arXiv:2205.13777 \[astro-ph.CO\]](#).
- [103] V. K. Oikonomou and E. C. Lymperiadou, “Effects of a Geometrically Realized Early Dark Energy Era on the Spectrum of Primordial Gravitational Waves,” *Symmetry* **14** no. 6, (2022) 1143, [arXiv:2206.00721 \[gr-qc\]](#).
- [104] T. L. Smith, M. Lucca, V. Poulin, G. F. Abellan, L. Balkenhol, K. Benabed, S. Galli, and R. Murgia, “Hints of early dark energy in Planck, SPT, and ACT data: New physics or systematics?,” *Phys. Rev. D* **106** no. 4, (2022) 043526, [arXiv:2202.09379 \[astro-ph.CO\]](#).
- [105] F. Niedermann and M. S. Sloth, “Hot new early dark energy,” *Phys. Rev. D* **105** no. 6, (2022) 063509, [arXiv:2112.00770 \[hep-ph\]](#).
- [106] F. Niedermann and M. S. Sloth, “Hot new early dark energy: Towards a unified dark sector of neutrinos, dark energy and dark matter,” *Phys. Lett. B* **835** (2022) 137555, [arXiv:2112.00759 \[hep-ph\]](#).
- [107] C.-F. Chang, “Imprint of early dark energy in stochastic gravitational wave background,” *Phys. Rev. D* **105** no. 2, (2022) 023508, [arXiv:2107.14258 \[astro-ph.CO\]](#).
- [108] V. I. Sabla and R. R. Caldwell, “Microphysics of early dark energy,” *Phys. Rev. D* **106** no. 6, (2022) 063526, [arXiv:2202.08291 \[astro-ph.CO\]](#).
- [109] L. Herold, E. G. M. Ferreira, and E. Komatsu, “New Constraint on Early Dark Energy from Planck and BOSS Data Using the Profile Likelihood,” *Astrophys. J. Lett.* **929** no. 1, (2022) L16, [arXiv:2112.12140 \[astro-ph.CO\]](#).
- [110] H. Wang and Y.-S. Piao, “Testing dark energy after pre-recombination early dark energy,” *Phys. Lett. B* **832** (2022) 137244, [arXiv:2201.07079 \[astro-ph.CO\]](#).

- [111] J.-Q. Jiang and Y.-S. Piao, “Toward early dark energy and $n_s=1$ with Planck, ACT, and SPT observations,” *Phys. Rev. D* **105** no. 10, (2022) 103514, [arXiv:2202.13379 \[astro-ph.CO\]](#).
- [112] H. Mohseni Sadjadi and V. Anari, “Early dark energy and the screening mechanism,” [arXiv:2205.15693 \[gr-qc\]](#).
- [113] A. Reeves, L. Herold, S. Vagnozzi, B. D. Sherwin, and E. G. M. Ferreira, “Restoring cosmological concordance with early dark energy and massive neutrinos?,” *Mon. Not. Roy. Astron. Soc.* **520** no. 3, (2023) 3688–3695, [arXiv:2207.01501 \[astro-ph.CO\]](#).
- [114] E. McDonough and M. Scalisi, “Towards Early Dark Energy in String Theory,” [arXiv:2209.00011 \[hep-th\]](#).
- [115] T. Simon, P. Zhang, V. Poulin, and T. L. Smith, “Updated constraints from the effective field theory analysis of BOSS power spectrum on Early Dark Energy,” [arXiv:2208.05930 \[astro-ph.CO\]](#).
- [116] H. Wang and Y.-S. Piao, “A fraction of dark matter faded with early dark energy?,” [arXiv:2209.09685 \[astro-ph.CO\]](#).
- [117] J. S. Cruz, F. Niedermann, and M. S. Sloth, “A grounded perspective on New Early Dark Energy using ACT, SPT, and BICEP/Keck,” [arXiv:2209.02708 \[astro-ph.CO\]](#).
- [118] M. Trodden, “Coupled Early Dark Energy,” 9, 2022. [arXiv:2209.15046 \[astro-ph.CO\]](#).
- [119] S. Nakagawa, F. Takahashi, and W. Yin, “Early dark energy by dark Higgs, and axion-induced non-thermal trapping,” [arXiv:2209.01107 \[astro-ph.CO\]](#).
- [120] K. Murai, F. Naokawa, T. Namikawa, and E. Komatsu, “Isotropic cosmic birefringence from early dark energy,” [arXiv:2209.07804 \[astro-ph.CO\]](#).
- [121] L. Hart and J. Chluba, “Using the cosmological recombination radiation to probe early dark energy and fundamental constant variations,” *Mon. Not. Roy. Astron. Soc.* **519** no. 3, (2023) 3664–3680, [arXiv:2209.12290 \[astro-ph.CO\]](#).
- [122] S. Hayashi, T. Minoda, and K. Ichiki, “Constraints on the phase transition of early dark energy with the CMB anisotropies,” *JCAP* **05** (2023) 032, [arXiv:2210.03348 \[astro-ph.CO\]](#).
- [123] L. Herold and E. G. M. Ferreira, “Resolving the Hubble tension with early dark energy,” *Phys. Rev. D* **108** no. 4, (2023) 043513, [arXiv:2210.16296 \[astro-ph.CO\]](#).
- [124] T. Takahashi and S. Yamashita, “Big bang nucleosynthesis and early dark energy in light of the EMPRESS Yp results and the H_0 tension,” *Phys. Rev. D* **107** no. 10, (2023) 103520, [arXiv:2211.04087 \[astro-ph.CO\]](#).
- [125] M.-X. Lin, E. McDonough, J. C. Hill, and W. Hu, “Dark matter trigger for early dark energy coincidence,” *Phys. Rev. D* **107** no. 10, (2023) 103523, [arXiv:2212.08098 \[astro-ph.CO\]](#).
- [126] B. S. Haridasu, H. Khoraminezhad, and M. Viel, “Scrutinizing Early Dark Energy models through CMB lensing,” [arXiv:2212.09136 \[astro-ph.CO\]](#).
- [127] T. Rudelius, “Constraints on early dark energy from the axion weak gravity conjecture,” *JCAP* **01** (2023) 014, [arXiv:2203.05575 \[hep-th\]](#).
- [128] M. Maziashvili, “Inflaton-driven early dark energy,” *Astropart. Phys.* **145** (2023) 102792, [arXiv:2111.07288 \[astro-ph.CO\]](#).
- [129] L. Brissenden, K. Dimopoulos, and S. Sánchez López, “Non-oscillating Early Dark Energy and Quintessence from Alpha-Attractors,” [arXiv:2301.03572 \[astro-ph.CO\]](#).
- [130] M. Kamionkowski and A. G. Riess, “The Hubble Tension and Early Dark Energy,” [arXiv:2211.04492 \[astro-ph.CO\]](#).

- [131] P. G. Ferreira and M. Joyce, “Cosmology with a primordial scaling field,” *Phys. Rev.* **D58** (1998) 023503, [arXiv:astro-ph/9711102](#) [[astro-ph](#)].
- [132] S. Tsujikawa, “Quintessence: A Review,” *Class. Quant. Grav.* **30** (2013) 214003, [arXiv:1304.1961](#) [[gr-qc](#)].
- [133] T. Karwal and M. Kamionkowski, “Dark energy at early times, the Hubble parameter, and the string axiverse,” *Phys. Rev.* **D94** no. 10, (2016) 103523, [arXiv:1608.01309](#) [[astro-ph.CO](#)].
- [134] M. S. Turner, “Coherent Scalar Field Oscillations in an Expanding Universe,” *Phys. Rev.* **D28** (1983) 1243.
- [135] B. Ratra and P. J. E. Peebles, “Cosmological Consequences of a Rolling Homogeneous Scalar Field,” *Phys. Rev.* **D37** (1988) 3406.
- [136] A. R. Liddle and R. J. Scherrer, “A Classification of scalar field potentials with cosmological scaling solutions,” *Phys. Rev.* **D59** (1999) 023509, [arXiv:astro-ph/9809272](#) [[astro-ph](#)].
- [137] S. Dutta and R. J. Scherrer, “Evolution of Oscillating Scalar Fields as Dark Energy,” *Phys. Rev.* **D78** (2008) 083512, [arXiv:0805.0763](#) [[astro-ph](#)].
- [138] J. S. W. Wong, “On the generalized emden-fowler equation,” *SIAM Review* **17** no. 2, (1975) 339–360. <http://www.jstor.org/stable/2029180>.
- [139] K. D. Lozanov and M. A. Amin, “Self-resonance after inflation: oscillons, transients and radiation domination,” *Phys. Rev.* **D97** no. 2, (2018) 023533, [arXiv:1710.06851](#) [[astro-ph.CO](#)].
- [140] M. C. Johnson and M. Kamionkowski, “Dynamical and Gravitational Instability of Oscillating-Field Dark Energy and Dark Matter,” *Phys. Rev.* **D78** (2008) 063010, [arXiv:0805.1748](#) [[astro-ph](#)].
- [141] J. Lesgourgues, “The Cosmic Linear Anisotropy Solving System (CLASS) I: Overview,” *arXiv e-prints* (Apr, 2011) [arXiv:1104.2932](#), [arXiv:1104.2932](#) [[astro-ph.IM](#)].
- [142] D. Blas, J. Lesgourgues, and T. Tram, “The Cosmic Linear Anisotropy Solving System (CLASS). Part II: Approximation schemes,” *Journal of Cosmology and Astro-Particle Physics* **2011** (Jul, 2011) 034, [arXiv:1104.2933](#) [[astro-ph.CO](#)].
- [143] T. Brinckmann and J. Lesgourgues, “MontePython 3: boosted MCMC sampler and other features,” [arXiv:1804.07261](#) [[astro-ph.CO](#)].
- [144] B. Audren, J. Lesgourgues, K. Benabed, and S. Prunet, “Conservative Constraints on Early Cosmology: an illustration of the Monte Python cosmological parameter inference code,” *JCAP* **1302** (2013) 001, [arXiv:1210.7183](#) [[astro-ph.CO](#)].
- [145] A. Gómez-Valent, “Fast test to assess the impact of marginalization in Monte Carlo analyses and its application to cosmology,” *Phys. Rev. D* **106** no. 6, (2022) 063506, [arXiv:2203.16285](#) [[astro-ph.CO](#)].
- [146] **Planck** Collaboration, N. Aghanim *et al.*, “Planck 2015 results. XI. CMB power spectra, likelihoods, and robustness of parameters,” *Astron. Astrophys.* **594** (2016) A11, [arXiv:1507.02704](#) [[astro-ph.CO](#)].
- [147] Planck Collaboration, P. A. R. Ade, N. Aghanim, M. Arnaud, M. Ashdown, J. Aumont, C. Baccigalupi, A. J. Banday, R. B. Barreiro, J. G. Bartlett, and *et al.*, “Planck 2015 results. XV. Gravitational lensing,” *A&A* **594** (Sept., 2016) A15, [arXiv:1502.01591](#).
- [148] **BOSS** Collaboration, S. Alam *et al.*, “The clustering of galaxies in the completed SDSS-III Baryon Oscillation Spectroscopic Survey: cosmological analysis of the DR12 galaxy sample,” *Mon. Not. Roy. Astron. Soc.* **470** no. 3, (2017) 2617–2652, [arXiv:1607.03155](#) [[astro-ph.CO](#)].

- [149] F. Beutler, C. Blake, M. Colless, D. H. Jones, L. Staveley-Smith, L. Campbell, Q. Parker, W. Saunders, and F. Watson, “The 6dF Galaxy Survey: baryon acoustic oscillations and the local Hubble constant,” *Mon. Not. R. Astron. Soc.* **416** (Oct., 2011) 3017–3032, [arXiv:1106.3366](#).
- [150] A. J. Ross, L. Samushia, C. Howlett, W. J. Percival, A. Burden, and M. Manera, “The clustering of the SDSS DR7 main Galaxy sample - I. A 4 per cent distance measure at $z = 0.15$,” *Mon. Not. R. Astron. Soc.* **449** (May, 2015) 835–847, [arXiv:1409.3242](#).
- [151] D. Camarena and V. Marra, “On the use of the local prior on the absolute magnitude of Type Ia supernovae in cosmological inference,” *Mon. Not. Roy. Astron. Soc.* **504** (2021) 5164–5171, [arXiv:2101.08641 \[astro-ph.CO\]](#).
- [152] G. Efstathiou, “To H_0 or not to H_0 ?,” *Mon. Not. Roy. Astron. Soc.* **505** no. 3, (2021) 3866–3872, [arXiv:2103.08723 \[astro-ph.CO\]](#).
- [153] D. M. Scolnic *et al.*, “The Complete Light-curve Sample of Spectroscopically Confirmed SNe Ia from Pan-STARRS1 and Cosmological Constraints from the Combined Pantheon Sample,” *Astrophys. J.* **859** no. 2, (2018) 101, [arXiv:1710.00845 \[astro-ph.CO\]](#).
- [154] S. Vagnozzi, “Consistency tests of Λ CDM from the early integrated Sachs-Wolfe effect: Implications for early-time new physics and the Hubble tension,” *Phys. Rev. D* **104** no. 6, (2021) 063524, [arXiv:2105.10425 \[astro-ph.CO\]](#).
- [155] Z. Hou, R. Keisler, L. Knox, M. Millea, and C. Reichardt, “How massless neutrinos affect the cosmic microwave background damping tail,” *Phys. Rev. D* **87** no. 8, (Apr., 2013) 083008, [arXiv:1104.2333 \[astro-ph.CO\]](#).
- [156] **HSC** Collaboration, C. Hikage *et al.*, “Cosmology from cosmic shear power spectra with Subaru Hyper Suprime-Cam first-year data,” [arXiv:1809.09148 \[astro-ph.CO\]](#).
- [157] N. A. Ignatyuk, S. L. Ogarkov, and D. V. Skliannyi, “Nonlocal Fractional Quantum Field Theory and Converging Perturbation Series,” *Symmetry* **15** (2023) 1823, [arXiv:2303.16011 \[hep-th\]](#).
- [158] H. Akaike, “A New Look at the Statistical Model Identification,” *IEEE Transactions on Automatic Control* **19** (1974) 716–723.
- [159] G. Efstathiou and P. Lemos, “Statistical inconsistencies in the KiDS-450 data set,” *Mon. Not. Roy. Astron. Soc.* **476** no. 1, (2018) 151–157, [arXiv:1707.00483 \[astro-ph.CO\]](#).
- [160] R. C. Nunes and S. Vagnozzi, “Arbitrating the S8 discrepancy with growth rate measurements from redshift-space distortions,” *Mon. Not. Roy. Astron. Soc.* **505** no. 4, (2021) 5427–5437, [arXiv:2106.01208 \[astro-ph.CO\]](#).
- [161] B. E. Robertson, R. S. Ellis, S. R. Furlanetto, and J. S. Dunlop, “Cosmic Reionization and Early Star-forming Galaxies: a Joint Analysis of new Constraints From Planck and the Hubble Space Telescope,” *Astrophys. J.* **802** no. 2, (2015) L19, [arXiv:1502.02024 \[astro-ph.CO\]](#).
- [162] C. Umiltà, M. Ballardini, F. Finelli, and D. Paoletti, “CMB and BAO constraints for an induced gravity dark energy model with a quartic potential,” *JCAP* **1508** (2015) 017, [arXiv:1507.00718 \[astro-ph.CO\]](#).
- [163] M. Ballardini, F. Finelli, C. Umiltà, and D. Paoletti, “Cosmological constraints on induced gravity dark energy models,” *JCAP* **1605** no. 05, (2016) 067, [arXiv:1601.03387 \[astro-ph.CO\]](#).
- [164] V. Poulin, Nov., 2018. https://github.com/PoulinV/class_EDE.